Biological impact of Pd(II) complexes: Synthesis, crystal structure, Hirshfeld surface analysis, NCI-RDG, molecular docking, molecular dynamic simulations

G. Samia, D. Ben Salah, B. Yamina, M. O. Zouaghi, Y. Arfaoui, L. Mansour, Mathieu Sauthier, N. Hamdi

Biological Impact of Pd(II) complexes: Synthesis, crystal structure, Hirshfeld surface analysis, NCI-RDG, molecular docking, molecular dynamic simulations

Guerfi Samiaa, [1,] [2]Donia Ben Salah[3], Berredjem Yamina[1,2,4], Mohamed Oussama Zouaghi [5], Youssef Arfaoui[5], lamjed Mansour[6] , Mathieu Sauthier [7]and Naceur Hamdi[3*]

[1] Faculté de technologie, Département de génie des procédés et de pétrochimie, université 20 août 1955Skikda.

[2] Laboratoire des sciences et technologies de l'eau et de l'environnement, Faculté des sciences et technologies, Département des sciences des matières, Université Mohammed Cherif Messaadia, Souk_ Aharas 41000. Algérie.

[3]Research Laboratory of Environmental Sciences and Technologies (LR16ES09), Higher Institute of Environmental Sciences and Technology, University of Carthage, Hammam-Lif, Tunisia

[4] Laboratoire de Traitement des Eaux et de Valorisation des Déchets Industriels, Faculté des Sciences, Département de Chimie, Université Badji-Mokhtar, B.P.12, Annaba 23000, Algérie.

[5]Laboratory of Characterizations, Applications & Modeling of Materials (LR18ES08), Department of Chemistry, Faculty of Sciences of Tunis, University of Tunis El Manar, 2092, Tunisia

[6] Zoology Department, College of Science, King Saud University, Saudi Arabia, P.O. Box 2455, Riyadh 11451, Saudi Arabia

Ecole Nationale Superieure de Chimie de Lille, Unite de Catalyse et Chimie du Solide, Villeneuve d'Ascq, France

Corresponding author: *E-Mail: hamdi.naceur@isste.ucar.tn, Tel: +21698503980

Abstract:

This work includes the synthesis of a new series of palladium-N-heterocyclic carbene complexes (**3a-i**). The new complexes were characterized using NMR (^{1}H and ^{13}C), FTIR spectroscopic, and elemental analysis techniques. The crystal structure of complex **3a** was obtained by utilizing the single- crystal X- ray diffraction method. X- ray studies show that the coordination environment of palladium atom is completed by the carbene atom of the NHC ligand, the nitrogen atom of the morpholine ring, and a pair of bromide ligand, resulting in the formation of slightly distorted square planar geometry. In order to gain more insight about structure the study also delved into the examination of various intermolecular interactions between neighboring molecules using Hirshfeld surfaces. A good agreement between experimental and theoretical data was observed. Furthermore, the antioxidant and the cytotoxicity activities of these compounds were assessed.

Density Functional Theory (DFT) calculations showed that PEPPSI-type palladium(II)-NHC complexes (**3a-i**) are structurally stable with bond lengths like Pd1-C1 ranging from 1.980–1.983 Å and a HOMO-LUMO gap of about 3.55 eV, suggesting potential for biological applications. Molecular docking and ADMET analyses indicated strong binding to Keap1 (-190.22 to -211.96) but weaker affinity for CDK2 (-129.04 to -136.57), with high lipophilicity (log P: 4.869-5.069) and toxicity risks highlighting the need for optimization.

Keywords: Strucutre analysis; Palladium, benzimidazol-2-ylidene; antibacterial properties; metallodrugs, MIC; Metallodrug design; Computational pharmacology

1-Introduction

An N-heterocyclic carbene (NHC) is a cyclic compound bearing at least one nitrogen atom bound to the carbene. The steric and electronic properties of the substituents attached to the nitrogen atom determine the stability and isolation of N-heterocyclic carbenes (NHCs)[1,2]. Additionally, NHCs are excellent σ-donor ligands but weak π-acceptors.[3-7] The electron-donating ability of NHCs depends on the type of metal, the nature of substituents attached to the nitrogen atoms, and other groups present on the NHC ring [8-10]. Owing to the stability of metal-NHC bonds, NHC-metal complexes are extensively studied [11,12]. Due to the properties discussed above, many studies are showing that metal-NHC complexes have catalytic and biological activity[13-19]. One class of metal-NHC complexes with palladium is the PEPPSI-type (Pyridine-Enhanced Precatalyst, Preparation, Stabilization, and Initiation) complex. These complexes, characterized by a bulky NHC ligand, two halides, and a pyridine-based ligand coordinated to palladium, were first reported by Organ in the literature [20]. Although some metal-NHC complexes can be expensive, sensitive to air and moisture, and challenging to synthesize [21-25], PEPPSI-type complexes overcome these limitations, making them widely preferred catalysts in C–C and C–heteroatom bond formation reactions. [26-29] The easy removal of pyridine in PEPPSI compounds from the structure during the catalytic cycle and the stability of the Pd- carbene bond provide these compounds with high catalytic activity.[30,31]

One of the most appealing properties of PEPPSI- Pd- NHC complexes in these studies is their stability in reaction environments under ambient conditions.[32] In the last decade, studies on the biological activities of the Pd- NHC complexes such as antileishmanial,[33] antibacterial, [17] antimicrobial,[34] and antitumor agents [35] have been published. Recently, studies on biological

activities of PEPPSI- Pd- NHC complexes have also been published such as cytotoxic activities against cancer cells, [36,37] DNA binding,[38] and enzyme inhibition effects. [39-43]

It is known that electronic and structural differences directly affect the catalytic activity of metal–NHC complexes. Moreover, studies on the biological activities of Ag(I)–, Au(I)– and Pd(II)–NHC complexes with different geometries show that the NHC ligand species are effective in kinetic properties such as the hydrolysis rates of molecules, and the kinetic stability is related to the structural properties of NHC rather than the central transition metal [44-45]. The bioavailability of metal–NHC complexes varies depending on the delivery method, solubility and ionization of metal ions [17-46]. Although it has not been fully elucidated yet, itis thought that metal ions could bind to the cell surface and interact with the cell membrane. Therefore, analysis of the electronic properties and electrochemical characterization of molecules can be considered as a useful method for future research. Density Functional Theory (DFT) has emerged as a cornerstone of computational chemistry, widely employed to analyze the structure, binding, and electronic properties of molecules. Recent advancements in the theoretical analysis of inorganic species have been particularly noteworthy [47–48], offering unprecedented precision in understanding complex systems such as metal-containing compounds. Complementing DFT, molecular docking methods provide detailed insights into how molecules interact with biological species at the atomic level [49-51]. These computational tools are especially relevant to PEPPSI-type palladium(II)-N-heterocyclic carbene (NHC) complexes, which are well-known for their catalytic applications in organic synthesis. However, their potential bioactivity has begun to attract interest. While studies in the literature report their antioxidant, enzyme inhibition, and antibacterial activities, broader bioactivity applications remain underexplored. This gap presents an exciting opportunity to harness computational techniques to investigate their therapeutic potential beyond their established catalytic roles.

The molecular docking technique is particularly valuable for modeling the interactions between a small compound (ligand) and protein targets at the atomic level. By predicting the orientation and binding affinity of ligands within the active sites of target proteins, docking illuminates key biochemical processes that these compounds may influence [52]. The method involves two fundamental steps: (1) describing the conformation of the ligand and (2) evaluating its binding relationship with the target.

Keeping in view the diversified significance of palladium(II) complexes in mind, we are describing the preparation, characterization, and biological potential of these complexes. The structures of these compounds were thoroughly characterized using spectroscopic methods, and their purity was confirmed through elemental analysis. Cytotoxic studies of these complexes were

carried out to examine its potential against cell lines to evaluate its pharmacological significance. Furthermore, the antioxidant activity of the palladium(II) complexes was investigated against 2,2-diphenyl-1-picrylhydrazyl (DPPH) which was found to be dosage dependent. By integrating experimental synthesis with advanced computational approaches like DFT and molecular docking, we aim to elucidate the structural, electronic, and biological properties of these complexes, potentially unlocking their promise as innovative metallodrugs. Further confirmations of complex 3a were provided by X-ray crystallography technique.

2-Experimental

2-1-Materials and Methods

All manipulations were carried out in air. All chemicals and solvents were purchased from Sigma-Aldrich and Merck. The solvents such as dimethylformamide (DMF), dichloromethane and diethyl ether were purified by distillation over the drying agents. Melting points were determined with an Electrothermal-9200 melting points apparatus. Fourier transform infrared spectra were obtained in the range 450-4000 cm^{-1} on a Perkin Elmer Spectrum 100 Spectrophotometer. The mass analysis was determined by using a Thermo Scientific Exactive Plus Benchtop Full-Scan Orbitrap Mass Spectrometer LC-MS/MS analyzer. ^{1}H NMR and ^{13}C NMR spectra were recorded at 400 MHz (1H), 100 MHz (^{13}C) in $CDCl_3$ with tetramethylsilane as an internal reference (Malaty, Turkey). The NMR studies were carried out in high-quality 5 mm NMR tubes. Signals are quoted in parts per million as δ downfield from tetramethylsilane (δ = 0.00) as an internal standard. NMR multiplicities are abbreviated as follows: s = singlet, d = doublet, t = triplet, m = multiplet. In the investigation of antimicrobial properties of palladium-NHCs, some microorganisms defined in the American Type Culture Collection (ATCC) were preferred.

Preparation of benzimidazolium salts 2

The reaction of 1-(2-morpholinoethyl)-5,6-dimethylbenzimidazole (1 mmol) with various alkyl chlorides or alkyl bromides (1.04 mmol) in toluene (10 mL) at 80°C for 72 hours afforded benzimidazole salts. A white solid was obtained after the addition of diethyl ether (15 mL), which was subsequently filtered off. After washing with diethyl ether (3 × 15 mL), the solid was dried under vacuum.

1-(2-Morpholinoethyl)-3-(2,3,5,6-tetramethylbenzyl)-5,6-dimethylbenzimidazolium chloride 2a

Yield: 90%; m.p. 256°C; IR (cm^{-1}): (C–N)=1556; CH (arom)=3020,CH(aliph)=2910; (C–O)=1203; HR-AM (H-ESI II) analysis calculated *(m/z)* for cationic part of $[C_{26}H_{36}N_3O]^+$: 406.59; found *(m/z)*: 406.2801. ^{1}H NMR (400 MHz, $CDCl_3$, 25) δ (ppm) = 2.25 (d, 12H, $CH_{3(c,d,e,f)}$), 2.37 (s, 3H, $CH_{3(b)}$), 2.41 (s, 3H, $CH_{3(a)}$), 2.47 (s, 4H, $H_{4',8'}$), 2.73 (s, 2H, $H_{2'}$), 3.40 (s, 4H, $H_{5',7'}$), 4.82 (s, 2H, $H_{1'}$), 5.63 (s, 2H, $H_{1''}$), 7.08 (s, 1H, $H_{5''}$); 7.24 (s,

1H, H_4), 7.45 (s, 1H, H_7), 10.16 (s, 1H, H_2); ^{13}C NMR (100 MHz, $CDCl_3$) δ (ppm) = 16.22 ($C_{c,f}$), 20.68 (C_a), 20.77 (C_b), 20.90 ($C_{d,e}$), 44.03 ($C_{1'}$), 46.66 ($C_{1''}$), 53.34 ($C_{4',8'}$), 56.10 ($C_{2'}$), 66.84 ($C_{5',7'}$), 112.74 (C_4), 113.01 (C_7), 127.96 ($C_{5''}$), 129.85 ($C_{8,9}$), 130.00 ($C_{4'',6''}$),133.68 ($C_{3'',7''}$), 134.10 (C_6), 135.28 (C_5), 137.04 ($C_{2''}$), 142.43 (C_2).

1-(2-Morpholinoethyl)-3-(2,3,4,5,6-pentamethylbenzyl)-5,6-dimethylbenzimidazolium chloride 2b

Yield: 83%; m.p. 250°C; IR (cm^{-1}): (CN) =1557; (C–N)=1294; CH (arom)=3163,CH(aliph)=2968; (C–O)=1223; HR-AM (H-ESI II) analysis calculated *(m/z)* for cationic part of $[C_{27}H_{38}N_3O]^+$: 420.62; found *(m/z)*: 420.2951. ^{1}H NMR (400 MHz, $CDCl_3$) δ (ppm) = 2.24 (s, 6H, $CH_{3(c,g)}$), 2.26 (s, 3H, $CH_{3(e)}$), 2.29 (s, 6H, $CH_{3(d,f)}$), 2.38 (s, 3H, $CH_{3(b)}$), 2.42 (s, 3H, $CH_{3(a)}$), 2.45 (s, 4H, $H_{4',8'}$), 2.71 (s, 2H, $H_{2'}$), 3.36 (s, 4H, $H_{5',7'}$), 4.83 (s, 2H, $H_{1'}$); 5.61 (s, 2H, $H_{1''}$), 7.31 (s, 1H, H_4), 7.47 (s, 1H, H_7), 9.94 (s, 1H, H_2); ^{13}C NMR (100 MHz, $CDCl_3$) δ (ppm) = 17.09 ($C_{c,g}$), 17.20 (C_e), 17.39 ($C_{d,e}$), 20.76 (C_a), 20.88 (C_b), 44.05 ($C_{1'}$), 47.02 ($C_{1''}$), 53.30 ($C_{4',8'}$), 56.12 ($C_{2'}$), 66.74 ($C_{5',7'}$), 112.80 (C_4), 112.91 (C_7), 125.25 ($C_{5''}$), 129.79 (C_8), 130.06 (C_9), 133.57 ($C_{4'',6''}$), 134.09 ($C_{3'',7''}$), 134.09 (C_6), 137.01 (C_5), 137.50 ($C_{2''}$), 142.16(C_2)

3-(Cyclobutylmethyl)-1-(2-morpholinoethyl)- 5,6-dimethylbenzimidazolium bromide 2c

Yield: 72%; m.p. 219°C; IR (cm^{-1}): (C–N)=562; CH (arom)= 3066,CH(aliph)=2938; (C–O)= 1223.; HR-AM (H-ESI II) analysis calculated *(m/z)* for cationic part of $[C_{20}H_{30}N_3O]^+$: 328.48; found *(m/z)*: 328.2341. ^{1}H NMR (400 MHz, $CDCl_3$) δ (ppm) = 1.90-1.98 (m, 4H, $H_{3'',5''}$), 2.11-2.16 (m, 2H, $H_{4''}$), 2.45 (s, 6H, $CH_{3(a,b)}$), 2.69 (s, 4H, $H_{4',8'}$), 3.00-3.06 (m, 2H, $H_{2'}$), 3.65 (s, 4H, $H_{5',7'}$), 4.49 (d, 2H, $H_{1'}$), 4.81 (t, 2H, $H_{1''}$), 7.41 (s, 1H, H_4); 7.54 (s, 1H, H_7), 11.03 (s, 1H, H_2), ^{13}C NMR (100 MHz, $CDCl_3$) δ (ppm) = 18.07 ($C_{4''}$), 20.81 ($C_{a,b}$), 25.85 ($C_{3'',5''}$), 34.39 ($C_{2''}$), 43.71 ($C_{1'}$), 52.02 ($C_{4',8'}$), 53.43 ($C_{2'}$), 56.04 ($C_{1''}$), 66.67 ($C_{5',7'}$), 112.80 (C_4), 112.84 (C_7), 129.76 (C_8),129.80 (C_9), 137.32 (C_6), 137.45 (C_5), 142.07 (C_2).

3-(4-Chlorobenzyl)-1-(2-morpholinoethyl)-5,6-dimethylbenzimidazolium chloride 2d

Yield: 73%; m.p. 244°C; ν (CN) = 1563 cm^{-1}; HR-AM (H-ESI II) analysis calculated *(m/z)* for cationic part of $[C_{22}H_{27}ClN_3O]^+$: 384.93; found *(m/z)*: 384.1787. ^{1}H NMR (400 MHz, $CDCl_3$) δ (ppm) = 2.38 (d, 6H, $CH_{3(a,b)}$), 2.59 (s, 4H, $H_{4',8'}$), 2.93 (s, 2H, $H_{2'}$), 3.62 (s, 4H, $H_{5',7'}$), 4.67 (s, 2H, $H_{1'}$), 5.80 (s, 2H, $H_{1''}$), 7.31 (t, 3H, $H_{4,3'',7''}$); 7.46 (d, 3H, $H_{7,4'',6''}$), 11.61 (s, 1H, H_2); ^{13}C NMR (100 MHz, $CDCl_3$) δ (ppm) = 20.80 (C_b), 20.82 (C_a), 44.13 ($C_{1'}$), 50.24 ($C_{4',8'}$), 53.44 ($C_{2'}$), 56.09 ($C_{1''}$), 66.86 ($C_{5',7'}$), 112.76 (C_4), 113.23 (C_7), 129.46 ($C_{8,9}$), 129.57 ($C_{3'',7''}$), 129.74 (C_6),129.91 (C_5), 131.88 ($C_{4'',6''}$), 135.25 ($C_{5''}$), 137.48 ($C_{2''}$), 143.27 (C_2).

3-Benzyl -1-(2-morpholinoethyl)-5,6-dimethylbenzimidazolium chloride 2e

Yield: 77%; m.p. 244°C; IR (cm^{-1}): (C–N)=1566; CH (arom)=3015,CH(aliph)=2934; (C–O)=1206; HR-AM (H-ESI II) analysis calculated *(m/z)* for cationic part of $[C_{22}H_{28}N_3O]^+$: 350.49; found *(m/z)*: 350.2181. ^{1}H NMR (400 MHz, $CDCl_3$) δ (ppm) = 2.38 (d, 6H, $CH_{3(a,b)}$), 2.56 (s, 4H, $H_{4',8'}$), 2.90 (s, 2H, $H_{2'}$), 3.59 (s, 4H, $H_{5',7'}$),

4.69 (s, 2H, $H_{1'}$), 5.75 (s, 2H, $H_{1''}$), 7.33 (t, 4H, $H_{4,4'',5'',6''}$); 7.46 (d, 3H, $H_{3'',7'',7}$), 11.57 (s, 1H, H_2); ^{13}C NMR (100 MHz, $CDCl_3$) δ (ppm) = 20.77 ($C_{a,b}$), 44.25 ($C_{1'}$), 50.97 ($C_{4',8'}$), 53.50 ($C_{2'}$), 56.19 ($C_{1''}$), 67.00 ($C_{5',7'}$), 112.71 (C_4), 113.33 (C_7), 128.16 ($C_{5''}$), 129.20 ($C_{4'',6''}$), 129.40 ($C_{8,9}$), 129.63 ($C_{3'',7''}$),,129.93 (C_6), 133.35 (C_5), 137.26 ($C_{2''}$), 143.30 (C_2).

3-(2-Methoxyethyl)-1-(2-morpholinoethyl)-5,6-dimethylbenzimidazolium chloride 2f

Yield: 91%; m.p. 160°C; IR (cm^{-1}): (C–N)=1566; CH (arom)=3020,CH(aliph)=2935; (C–O)=1207; HR-AM (H-ESI II) analysis calculated *(m/z)* for cationic part of $[C_{18}H_{28}N_3O_2]^+$: 318.44; found *(m/z)*: 318.2121. ^{1}H NMR (400 MHz, $CDCl_3$) δ (ppm) = 2.43 (s, 6H, $CH_{3(a,b)}$), 2.65 (s, 4H, $H_{4',8'}$), 2.98(s, 2H, $H_{2'}$), 3.34 (s, 3H, $CH_{3(4'')}$), 3.67 (s, 4H, $H_{5',7'}$), 3.92 (t, 2H, $H_{2''}$), 4.70 (t, 4H, $H_{1', 1''}$), 7.49 (s, 2H, $H_{4,7}$), 11.15 (s, 1H, H_2); ^{13}C NMR (100 MHz, $CDCl_3$) δ (ppm) = 20.74 ($C_{a,b}$), 47.47 ($C_{1'}$), 53.24 ($C_{2',4',8'}$), 59.18 ($C_{1',4''}$), 70.21 ($C_{2'',5',7'}$), 112.63 (C_7), 113.26 (C_8), 113.44 (C_9), 129.63 (C_4), 130.40 (C_6), 137.18 (C_5), 142.89 (C_2).

3-(2-Ethoxyethyl)-1-(2-morpholinoethyl)-5,6-dimethylbenzimidazolium chloride 2g

Yield: 92%; m.p. 109°C; IR (cm^{-1}): (C–N)=1563; CH (arom)=3022,CH(aliph)=2933; (C–O)=1210; HR-AM (H-ESI II) analysis calculated *(m/z)* for cationic part of $[C_{19}H_{28}N_3O_2]^+$: 332.47; found *(m/z)*: 332.2278. ^{1}H NMR (400 MHz, $CDCl_3$) δ (ppm) = 1.09 (t, 3H, $CH_{3(5'')}$), 2.42 (d, 6H, $CH_{3(a,b)}$), 2.84 (s, 4H, $H_{4',8'}$), 3.21 (s, 2H, $H_{2'}$), 3.49 (q, 2H, $H_{4''}$), 3.76 (s, 4H, $H_{5',7'}$), 3.92 (t, 2H, $H_{2''}$), 4.67 (t, 2H, $H_{1'}$), 4.91 (s, 2H, $H_{1''}$), 7.53 (s, 1H, H_4); 7.63 (s, 1H, H_7), 11.08 (s, 1H, H_2); ^{13}C NMR (100 MHz, $CDCl_3$) δ (ppm) = 14.87 ($C_{5''}$), 20.50 (C_b), 20.56 (C_a), 47.74($C_{1'}$), 52.90 ($C_{2',4',8'}$), 66.73 ($C_{1''}$), 68.10 ($C_{5',7',2'',4''}$), 112.49 (C_7), 113.65 (C_4), 129.48 ($C_{8,9}$), 130.30 (C_6), 136.95 (C_5), 142.51 (C_2).

3-(3,5-Di-tert-butylbenzyl)-1-(2-morpholinoethyl)-5,6-dimethylbenzimidazolium bromide 2h

Yield: 92%; m.p. 247°C; IR (cm^{-1}): (C–N)=1564; CH (arom)=3023,CH(aliph)=2937; (C–O)=1210; HR-AM (H-ESI II) analysis calculated *(m/z)* for cationic part of $[C_{30}H_{44}N_3O]^+$: 462.71; found *(m/z)*: 462.3415. ^{1}H NMR (400 MHz, $CDCl_3$) δ (ppm) = 1.28 (s, 18H, $CH_{3(c,d,e,f,g,h)}$), 2.37 (s, 3H, $CH_{3(b)}$), 2.42 (s, 3H, $CH_{3(a)}$), 2.57 (s, 4H, $H_{4',8'}$), 2.93 (s, 2H, $H_{2'}$), 3.56 (s, 4H, $H_{5',7'}$), 4.72 (t, 2H, $H_{1'}$), 5.68 (s, 2H, $H_{1''}$), 7.29 (d, 2H, $H_{3'',7''}$); 7.36 (s, 1H, H_4), 7.41 (s, 1H, $H_{5''}$), 7.46 (s, 1H, H_7), 11.17 (s, 1H, H_2); ^{13}C NMR (100 MHz, $CDCl_3$) δ (ppm) = 20.79 (C_b), 20.81 (C_a), 31.50 ($C_{c,d,e,f,g,h}$), 35.07 ($C_{8'',9''}$), 52.14 ($C_{1'}$), 53.44 ($C_{2',4',8''}$), 65.97 ($C_{1'',5',7'}$), 112.86 (C_4), 113.57 (C_7), 122.84 ($C_{5''}$), 123.42 ($C_{4'',6''}$), 129.76 (C_8),130.14 (C_9), 131.93 ($C_{3'',7''}$), 137.20 ($C_{5,6}$), 142.36 ($C_{2''}$), 152.29 (C_2).

3-(4-(Tert-butyl)benzyl)-1-(2-morpholinoethyl)-5,6-dimethylbenzimidazolium bromide 2i

Yield: 80%; m.p. 224°C; ν (CN) = IR (cm^{-1}): (C–N)=1557; CH (arom)=3010,CH(aliph)=2932; (C–O)=1208; HR-AM (H-ESI II) analysis calculated *(m/z)* for cationic part of $[C_{26}H_{36}N_3O]^+$: 406.60; found *(m/z)*: 406.2800. ^{1}H NMR (400 MHz, $CDCl_3$) δ (ppm) = 1.26 (s, 9H, $CH_{3(c,d,e)}$), 2.40 (d, 6H, $CH_{3(a,b)}$), 2.68 (s, 4H, $H_{4',8'}$), 3.02

(s, 2H, $H_{2'}$), 3.62 (s, 4H, $H_{5',7'}$), 4.81 (s, 2H, $H_{1'}$), 5.66 (s, 2H, $H_{1''}$), 7.40 (q, 5H, $H_{4,3'',4'',6'',7''}$), 7.56 (s, 1H, H_7); 11.08 (s, 1H, H_2); ^{13}C NMR (100 MHz, $CDCl_3$) δ (ppm) = 20.78 (C_b), 20.82 (C_a), 31.27 ($C_{c,d,e}$), 34.78 ($C_{8''}$), 50.78 ($C_{1'}$), 53.26 ($C_{4',8',2'}$), 55.73 ($C_{1''}$), 66.50 ($C_{5',7''}$), 112.87 (C_4), 113.25 (C_7), 126.43 ($C_{5''}$), 128.12 ($C_{4'',6''}$), 129.62 (C_8),129.86 (C_9), 129.99 ($C_{3'',7''}$), 137.43 ($C_{5,6}$), 142.34 ($C_{2''}$), 152.59 (C_2).

Synthesis of PEPPSI-Type Palladium NHC Complexes (3a-i)

A mixture benzimidazolium salts **2a-i** (1 eq) with $PdCl_2$,(1.05 eq), K_2CO_3 (5 eq), KBr (10 eq) and pyridine (1 eq) in the presence of acetonitrile was heated at 80 °C for 16 h. A short silica column was used for filtration. Then, the resulting complexes dried under vacuum. The yellow solid was crystallized from dichloromethane/*n*-pentane for further purification.

Dibromo-[1-(2-morpholinoethyl)-3-(2,3,5,6-tetramethylbenzyl)-5,6-dimethylbenzimidazole-2-ylidene](pyridine) palladium(II), 3a

Yield: 71%; m.p. 205°C; IR ν/cm^{-1} (C–N)=1445; CH (arom)=3005,CH(aliph)=2931; (C–O)=1201; HR-AM (H-ESI II) analysis calculated *(m/z)* [M-C_5H_5BrN]: 591,01; found *(m/z)*: 592.09106. ^{1}H NMR (400 MHz, $CDCl_3$) δ (ppm) = 2.10 (s, 3H, $CH_{3(b)}$), 2.23 (s, 6H, $CH_{3(c,f)}$), 2.26 (s, 6H, $CH_{3(d,e)}$), 2.30 (s, 3H, $CH_{3(a)}$), 2.76 (s, 4H, $H_{4',8'}$), 3.27 (s, 2H, $H_{2'}$), 3.77 (s, 4H, $H_{5',7'}$), 4.99 (s, 2H, $H_{1'}$), 6.03 (s, 2H, $H_{1''}$), 6.13 (s, 1H, $H_{5''}$); 7.11 (s, 1H, H_4), 7.21 (s, 1H, H_7), 7.34 (td, 2H, $H_{3''',5'''}$), 7.77 (td, 1H, $H_{4'''}$), 8.94 (dd, 2H, $H_{2''',6'''}$); ^{13}C NMR (100 MHz, $CDCl_3$) δ (ppm) = 16.83 ($C_{c,f}$), 20.31 (C_b), 20.53 (C_a), 20.73 ($C_{d,e}$), 50.74 ($C_{1',1'',4',8'}$), 53.97 ($C_{2',5',7'}$), 110.76 (C_4), 111.86 (C_7), 124.97 ($C_{3''',5'''}$), 130.86 ($C_{5''}$), 131.99 ($C_{8,9}$), 132.52 ($C_{4'',6''}$), 133.57 (C_5), 133.71 (C_6), 134.38 ($C_{3'',7''}$), 135.34 ($C_{4'''}$), 137.99 ($C_{2''}$), 152.59 ($C_{2''',6'''}$), 160.71 (C_2). Anal. Calc. for C31H40Br2N4OPd: C, 49.58%; H, 5.37%; N, 7.46%, found: C, 49.6; H, 5.4; N, 7.5%

Dibromo-[1-(2-morpholinoethyl)-3-(2,3,4,5,6-pentamethylbenzyl)-5,6-dimethylbenzimidazole-2-ylidene](pyridine) palladium(II), 3b

Yield:66%; m.p. 238°C; IR ν/cm^{-1}; (CN) =1439; (C–N)=1324; CH (arom)=3000,CH(aliph)=2884; (C–O)=1264; HR-AM (H-ESI II) analysis calculated *(m/z)* for [M- C_5H_5BrN]: 605,93; found *(m/z)*: 606.10718. ^{1}H NMR (400 MHz, $CDCl_3$) δ (ppm) = 2.07 (s, 3H, $CH_{3(e)}$), 2.24 (s, 6H, $CH_{3(d,f)}$), 2.28 (s, 6H, $CH_{3(c,g)}$) 2.30 (s, 3H, $CH_{3(b)}$), 2.34 (s, 3H, $CH_{3(a)}$), 2.77 (s, 4H, $H_{4',8'}$), 2.28 (s, 2H, $H_{2'}$), 3.78 (s, 4H,$H_{5',7'}$), 5.00 (s, 2H, $H_{1'}$); 6.06 (s, 2H, $H_{1''}$), 6.08 (s, 1H, H_4), 7.21 (s, 1H, H_7), 7.34(td, 2H, $H_{3''',5'''}$), 7.77 (td, 1H, $H_{4'''}$), 8.95 (dd, 2H, $H_{2''',6'''}$); ^{13}C NMR (100 MHz, $CDCl_3$) δ (ppm) = 17.04 ($C_{c,g}$), 17.38 (C_b), 17.83 (C_a), 20.29 ($C_{d,f}$), 20.55 (C_e), 51.47 ($C_{1',1'',4',8'}$), 53.96 ($C_{2',5',7'}$), 110.68 (C_4), 112.03 (C_7), 124.65 ($C_{3''',7'''}$), 128.15 ($C_{8,9}$), 133.17 ($C_{4'',6''}$), 133.62 (C_5), 133.75 (C_6), 134.94 ($C_{3'',7''}$), 136.01 ($C_{4'''}$), 137.98 ($C_{2''}$), 152.61 ($C_{2''',6'''}$), 160.52 (C_2). Anal. Calc. for C32H42Br2N4OPd: C, 50.25%; H, 5.53%; N, 7.32%, found: C, 50.1; H, 5.6; N, 7.35%

Dibromo-[3-(cyclobutylmethyl)-1-(2-morpholinoethyl)-1-(2-morpholinoethyl)-5,6-dimethylbenzimidazole-2-ylidene](pyridine) palladium(II), 3c

Yield:53%; m.p. 249°C; IR ν/cm^{-1}; (C–N)=1444; CH (arom)=2931,CH(aliph)=2931; (C–O)=1200; HR-AM (H-ESI II) analysis calculated *(m/z)* for [M- C_5H_5BrN]: 513,79; found *(m/z)*: 514.04468. ^{1}H NMR (400 MHz, $CDCl_3$) δ (ppm) = 1.93-2.20 (m, 7H, $H_{2'',3'',4'',5''}$), 2.38 (s, 6H, $CH_{3(a,b)}$), 2.76 (s, 4H, $H_{4',8'}$), 3.26 (s, 2H, $H_{2'}$), 3.76 (s, 4H, $H_{5',7'}$), 4.75 (d, 2H, $H_{1''}$), 4.97 (s, 2H, $H_{1'}$), 7.18 (s, 1H, H_4); 7.26 (s, 1H, H_7);7.37 (t, 2H, $H_{3''',5'''}$), 7.79 (td, 1H, $H_{4'''}$), 9.05 (dd, 2H, $H_{2''',6'''}$). ^{13}C NMR (100 MHz, $CDCl_3$) δ (ppm) = 18.51 ($C_{4''}$), 20.42 (C_b), 20.46 (C_a), 27.34 ($C_{3'',5''}$), 35.51 ($C_{2''}$), 53.90 ($C_{4',8',2'}$), 54.19 ($C_{1',1'',5',7'}$), 111.07 ($C_{4,7}$), 124.79 ($C_{3''',5'''}$), 133.50 ($C_{8,9}$), 133.68 ($C_{5,6}$), 138.12 ($C_{4'''}$),152.72 ($C_{2''',6'''}$), 159.75 (C_2). Anal. Calc. for C26H34Br2N3OPd: C, 46.55%; H, 5.11%; N, 6.26%, found: C, 46.6; H, 5.2; N, 6.3%.

Dibromo-[3-(4-chlorobenzyl)-1-(2-morpholinoethyl)-5,6-dimethylbenzimidazole-2-ylidene](pyridine) palladium(II), 3d

Yield: 46%; m.p. 130°C; ν IR ν/cm^{-1} (CN)=1446; (C–N)=1294; CH (arom)=3163,CH(aliph)=2968; (C–O)=1223;HR-AM (H-ESI II) analysis calculated *(m/z)* for [M- C_5H_5BrN]: 570.24; found *(m/z)*: 569.98999. ^{1}H NMR (400 MHz, $CDCl_3$) δ (ppm) = 2.16 (s, 3H, $CH_{3(a)}$), 2.27 (s, 3H, $CH_{3(b)}$), 2.69 (s, 4H, $H_{4',8'}$), 3.22 (s, 2H, $H_{2'}$), 3.69 (s, 4H, $H_{5',7'}$), 4.93 (s, 2H, $H_{1'}$), 5.98 (s, 2H, $H_{1''}$), 6.70 (s, 1H, H_4), 7.19 (s, 1H, H_7), 7.24-7.30 (m, 4H, $H_{3'',7'',4'',6''}$); 7.41 (d, 2H, $H_{3''',5'''}$), 7.70 (t, 1H, $H_{4'''}$), 8.93 (d, 2H, $H_{2''',6'''}$); ^{13}C NMR (100 MHz, $CDCl_3$) δ (ppm) = 20.39 (C_b), 20.44 (C_a), 52.72 ($C_{1',1''}$), 53.99 ($C_{4',8'}$), 56.95 ($C_{2'}$), 66.91 ($C_{5',7'}$), 111.22 (C_4), 111.61 (C_7), 124.78 ($C_{3''',5'''}$), 129.12 ($C_{3'',7''}$), 129.42 ($C_{4'',6''}$),132.82 ($C_{8,9}$), 133.67 ($C_{5''}$), 133.96 ($C_{5,6}$), 134.05 ($C_{2''}$), 138.17 ($C_{4'''}$), 152.68 ($C_{2''',6'''}$), 161.51 (C_2). Anal. Calc. for C27H31Br2ClN4OPd: C, 44.47%; H, 4.28%; N, 7.68%, found: C, 44.5; H, 4.3; N, 7.7%

Dibromo-[3-benzyl-1-(2-morpholinoethyl)-5,6-dimethylbenzimidazole-2-ylidene](pyridine) palladium(II), 3e

Yield: 70%; m.p. 228°C; IR ν/cm^{-1}; (C–N)=1417; CH (arom)= 3000,CH(aliph)=2918; (C–O)= 1261; HR-AM (H-ESI II) analysis calculated *(m/z)* for [M- C_5H_5BrN]: 535,80; found *(m/z)*: 536.02930. ^{1}H NMR (400 MHz, $CDCl_3$) δ (ppm) = 2.21 (s, 3H, $CH_{3(b)}$), 2.33 (s, 3H, $CH_{3(a)}$), 2.75 (s, 4H, $H_{4',8'}$), 3.28 (s, 2H, $H_{2'}$), 3.76 (t, 4H, $H_{5',7'}$), 4.99 (t, 2H, $H_{1'}$), 6.08 (s, 2H, $H_{1''}$), 6.79 (s, 1H, H_4); 7.24 (s, 1H, H_7), 7.31-7.38 (m, 5H, $H_{3'',4'',5'',6'',7''}$), 7.55 (d, 2H, $H_{3''',5'''}$), 7.76 (td, 1H, $H_{4'''}$), 9.02 (dd, 2H, $H_{2''',6'''}$); ^{13}C NMR (100 MHz, $CDCl_3$) δ (ppm) = 20.35 (C_b), 20.42 (C_a) 53.50 ($C_{1',1''}$), 54.05 ($C_{4',8'}$), 57.03 ($C_{2'}$), 67.03 ($C_{5',7'}$), 111.06 (C_4), 111.83 (C_7), 124.73 ($C_{3''',5'''}$), 128.12 ($C_{5''}$), 128.90 ($C_{3'',7''}$), 132.40 ($C_{4'',6''}$), 133.06 ($C_{8,9}$), 133.98 ($C_{5,6}$), 135.22 ($C_{4'''}$), 138.09 ($C_{2''}$), 152.70 ($C_{2''',6'''}$), 161.27 (C_2). Anal. Calc. for C27H32Br2N4OPd: C, 46.67%; H, 4.64%; N, 8.06%, found: C, 46.7; H, 4.7; N, 8.1%

Dibromo-[3-(2-methoxyethyl)-1-(2-morpholinoethyl)-5,6-dimethylbenzimidazole-2-ylidene](pyridine) palladium(II), 3f

Yield:63%; m.p. 210°C; IR ν/cm^{-1}; (C–N)=1446; CH (arom)=2906,CH(aliph)=2918; (C–O)=1209;HR-AM (H-ESI II) analysis calculated *(m/z)* for [M]$^+$: 662,76; found *(m/z)*: 662.98938. ^{1}H NMR (400 MHz, $CDCl_3$) δ

(ppm) = 2.27 (d, 6H, CH3a,b), 2.64 (s, 4H, $H_{4',8'}$), 3.15(s, 2H, $H_{2'}$), 3.25 (s, 3H, $H_{4''}$), 3.65 (s, 4H, $H_{5'',7''}$), 4.05 (t, 2H, $H_{2''}$), 4.83 (t, 4H, $H_{1',1''}$), 7.15 (s, 1H, H_4), 7.19 (s, 1H, H_7); 7.26 (t, 2H, $H_{3''',5'''}$), 7.68 (td, 1H, $H_{4'''}$), 8.94 (dd, 2H, $H_{2''',6'''}$); ^{13}C NMR (100 MHz, $CDCl_3$) δ (ppm) = 20.40 (C_a), 20.41 (C_b), 48.74 ($C_{1'}$), 53.91 ($C_{1''}$), 59.31 ($C_{2',4',8'}$), 65.98 ($C_{4'',5',7'}$), 71.35 ($C_{2''}$), 110.85 (C_4), 111.84 (C_7), 124.78 ($C_{3''',5'''}$), 132.47 ($C_{8,9}$), 133.39 (C_5), 134.23 (C_6), 138.16 ($C_{4'''}$), 152.73 ($C_{2''',6'''}$), 160.17 (C_2). Anal. Calc. for C23H32Br2N4O2Pd: C, 41.68%; H, 4.87%; N, 8.45%, found: C, 41.7; H, 4.9; N, 8.5%.

Dibromo-[3-(2-ethoxyethyl)-1-(2-morpholinoethyl)-5,6-dimethylbenzimidazole-2-ylidene](pyridine) palladium(II), 3g

Yield:52%; m.p. 175°C; IR ν/cm^{-1} ;(C–N)=1442; CH (arom)=2933,CH(aliph)=2918; (C–O)=1208

HR-AM (H-ESI II) analysis calculated *(m/z)* for [M- C_5H_5BrN]: 517.78; found *(m/z)*: 518.04059. ^{1}H NMR (400 MHz, $CDCl_3$) δ (ppm) = 1.14 (t, 3H, $CH_{3(5'')}$), 2.37 (d, 6H, $CH_{(a,b)}$), 2.70 (t, 4H, $H_{4',8'}$), 3.20 (t, 2H, $H_{2'}$), 3.51 (q, 2H, $H_{4''}$), 3.73 (t, 4H, $H_{5',7'}$), 4.16 (t, 2H, $H_{2''}$), 4.90 (t, 2H, $H_{1''}$), 4.96 (t, 2H, $H_{1'}$), 7.18 (s, 1H, H_4); 7.35-7.38 (m, 3H, $H_{7,3''',5'''}$), 7.78 (td, 1H, $H_{4'''}$), 9.05 (dd, 2H, $H_{2''',6'''}$); ^{13}C NMR (100 MHz, $CDCl_3$) δ (ppm) = 15.31 ($C_{5''}$), 20.31 (C_a), 20.42 (C_b), 46.15 ($C_{1'}$), 49.04 ($C_{1''}$), 54.11 ($C_{4',8'}$), 57.00 ($C_{',}$), 66.91 ($C_{4''}$), 67.15 ($C_{5',7'}$), 69.26 ($C_{2''}$), 110.70 (C_4), 112.21 (C_7), 124.75 ($C_{3''',5'''}$), 132.17 ($C_{8,9}$), 133.49 (C_5), 134.19 (C_6), 138.11 ($C_{4'''}$), 152.73 ($C_{2''',6'''}$), 160.05 (C_2). Anal. Calc. for C24H34Br2N4O2Pd: C, 42.59%; H, 5.06%; N, 8.28%, found: C, 42.6; H, 5.1; N, 8.3%.

Dibromo-[3-(3,5-di-tert-butylbenzyl)-1-(2-morpholinoethyl)-5,6-dimethylbenzimidazole-2-ylidene](pyridine) palladium(II), 3h

Yield: 62%; m.p. 137°C; IR ν/cm^{-1} (C–N)=1446; CH (arom)=2933,CH(aliph)=2951; (C–O)=1228; HR-AM (H-ESI II) analysis calculated *(m/z)* for $[M]^+$: 807,02; found *(m/z)*: 809.30591. ^{1}H NMR (400 MHz, $CDCl_3$) δ (ppm) = 1.23 (s, 18H, $CH_{3(c,d,e,f,g,h)}$), 2.13 (s, 3H, $CH_{3(b)}$), 2.27 (s, 3H, $CH_{3(a)}$), 2.70 (s, 4H, $H_{4',8'}$), 3.25 (s, 2H, $H_{2'}$), 3.69 (s, 4H, $H_{5',7'}$), 4.94 (s, 2H, $H_{1'}$), 6.00 (s, 2H, $H_{1''}$), 6.76 (s, 1H, $H_{5''}$); 7.19 (s, 1H, H_4), 7.28-7.30 (m, 3H, $H_{7,3'',5''}$), 7.36 (d, 2H, $H_{3''',7'''}$), 7.70 (td, 1H, $H_{4'''}$), 8.97 (dd, 2H, $H_{2''',6'''}$); ^{13}C NMR (100 MHz, $CDCl_3$) δ (ppm) = 20.35 (C_b), 20.41 (C_a), 31.62 ($C_{c,d,e,f,g,h}$), 35.11 ($C_{8'',9''}$), 53.96 ($C_{1',1'',4',8'}$), 54.44 ($C_{2',5',7'}$), 111.01 (C_4), 112.18 (C_7), 121.91 ($C_{3''',5'''}$), 122.95 ($C_{5''}$), 124.72 ($C_{4'',6''}$), 133.14 ($C_{3'',7''}$), 134.00 ($C_{8,9}$), 134.17 ($C_{5,6}$), 138.06 ($C_{4'''}$), 151.37 ($C_{2''}$), 152.74 ($C_{2''',6'''}$), 160.94 (C_2). Anal. Calc. for C35H48Br2N4OPd: C, 52.09%; H, 6.00%; N, 6.94%, found: C, 52.1; H, 6.0; N, 7.1%.

Dibromo-[3-(4-(tert-butyl)benzyl)-1-(2-morpholinoethyl)-5,6-dimethylbenzimidazole-2-ylidene](pyridine) palladium(II), 3i

Yield: 70%; m.p. 128°C; IR ν/cm^{-1} 1445 (C–N); CH (arom)=2933,CH(aliph)=2955; (C–O)=1208; HR-AM (H-ESI II) analysis calculated *(m/z)* for [M- C_5H_5BrN]: 591,91; found *(m/z)*: 592.09119. ^{1}H NMR (400 MHz, $CDCl_3$) δ (ppm) = 1.29 (s, 9H, $CH_{3(c,d,e)}$), 2.22 (s, 3H, $CH_{3(b)}$), 2.33 (s, 3H, $CH_{3(a)}$), 2.77 (s, 4H, $H_{4',8'}$), 3.30 (s,

2H, $H_{2'}$), 3.77 (s, 4H, $H_{5',7'}$), 5.01 (s, 2H, $H_{1'}$), 6.05 (s, 2H, $H_{1''}$), 6.82 (s, 1H, H_4), 7.33-7.38 (m, 5H, $H_{7,3'',4'',6'',7''}$), 7.50 (d, 2H, $H_{3''',5'''}$), 7.76 (td, 1H, $H_{4'''}$); 9.02 (dd, 2H, $H_{2''',6'''}$); ^{13}C NMR (100 MHz, $CDCl_3$) δ (ppm) = 20.34 (C_b), 20.42 (C_a), 31.45 ($C_{c,d,e}$), 34.70 ($C_{8''}$), 53.27 ($C_{1',1'',4',8'}$), 53.97 ($C_{2',5',7'}$), 111.04 (C_4), 111.95 (C_7), 124.72 ($C_{3''',5'''}$), 125.82 ($C_{4'',6''}$), 127.85 ($C_{3'',7''}$),132.13 ($C_{8,9}$), 133.08 ($C_{5,6}$), 133.95 ($C_{4'''}$), 138.09 ($C_{2''}$), 151.10 ($C_{5''}$), 152.71 ($C_{2''',6'''}$), 161.07 (C_2). Anal. Calc. for C31H40Br2N4OPd: C, 49.58%; H, 5.37%; N, 7.46%, found: C, 49.6; H, 5.4; N, 7.5%.

X-ray crystallography

X-ray diffraction data of complex **3a** were collected on a STOE IPDS II diffractometer at room temperature using graphite-monochromated Mo Kα radiation by applying the ω-scan method. Data collection and cell refinement were carried out using X-AREA [53] while data reduction was applied using X-RED32 [53]. The structure was solved by a dual-space algorithm using SHELXT-2018 [54] and refined by means of the full-matrix least-squares calculations on F^2 using SHELXL-2019 [55]. All H atoms were located in difference maps and then treated as riding atoms, fixing the bond lengths at 0.93, 0.97 and 0.96 Å for CH, CH_2 and CH_3 atoms, respectively. The displacement parameters of the H atoms were fixed at $U_{iso}(H) = 1.2U_{eq}$ ($1.5U_{eq}$ for CH_3). Crystal data, data collection and structure refinement details are collected in Table 1. Molecular graphic was created by using OLEX2 [56].

Table 1. Crystal data and structure refinement parameters for PEPPSI-Pd(II)–N-heterocyclic carbene (NHC) complex **3a**

CCDC depository	2294603
Color/shape	Yellow/prism
Chemical formula	$[PdBr_2(C_{26}H_{35}N_3O)(C_5H_5N)]$
Formula weight	750.89
Temperature (K)	296(2)
Wavelength (Å)	0.71073 Mo Kα
Crystal system	Monoclinic
Space group	*C*2/*c* (No. 15)
Unit cell parameters	
a, *b*, *c* (Å)	24.7681(12), 15.3486(11), 17.0756(11)
β (°)	100.464(4)
Volume (Å^3)	6383.4(7)
Z	8
$D_{calc.}$ (g/cm^3)	1.563
μ (mm^{-1})	3.115
Absorption correction	Integration
$T_{min.}$, $T_{max.}$	0.3240, 0.6781
F_{000}	3024
Crystal size (mm^3)	0.61 × 0.36 × 0.14
Diffractometer	STOE IPDS II

Measurement method	ω scan
Index ranges	$-27 \leq h \leq 31$, $-19 \leq k \leq 19$, $-21 \leq l \leq 21$
θ range for data collection (°)	$1.568 \leq \theta \leq 26.827$
Reflections collected	23981
Independent/observed reflections	6796/3840
Refinement method	Full-matrix least-squares on F^2
Data/restraints/parameters	6796/0/358
Goodness-of-fit on F^2	0.933
Final R indices [$I > 2\sigma(I)$]	$R_1 = 0.0487$, $wR_2 = 0.0815$
R indices (all data)	$R_1 = 0.1082$, $wR_2 = 0.0981$
$\Delta\rho_{max.}$, $\Delta\rho_{min.}$ (e/Å^3)	0.69, −0.84

Biological Activities

Anticancer (MTT) Test

Anticancer properties of the samples were reported by Sharma et al. (2019), it was evaluated against HCT116 (human colon cancer), SH-SY5Y (human brain cancer) and BEAS-2B (human healthy lung cell) cell lines. All cells were cultured in DMEM medium supplemented with 10% fetal bovine serum and 1% penicillin and streptomycin at 37 °C in a 5% CO atmosphere. After the cells covered the surface of the flask by 70-80%, the old medium was discarded and washed several times with sterile PBS (pH 7.4). Trypsin was then added and distributed evenly on the cell surfaces. After incubation with trypsin for 5 min at 37 °C, trypsin activity was inhibited by adding a 2 fold volume of fresh medium. The resulting solution was centrifuged at 1000 rpm for 7 minutes, and then the old medium was replaced with 5 mL of fresh medium. Cells were counted and diluted to obtain a final concentration of 1×10^5 cells/mL, then the cell solution was added to 96-well cell plate wells (1×10^4 cells/well). Plates containing cells were incubated at 37 °C in a 5% CO_2 atmosphere for 24 hours for cell attachment, and anticancer activity analyzes of the compounds were performed using the MTT method. For analysis, the test substance was diluted with fresh broth medium to obtain the desired concentration (0.8 – 800µg/ml) from the stock while the cells were incubated. The old medium was aspirated from the wells containing the cells and 100 µl of broth containing the test substance was added to the wells. The plates were then incubated at 37 °C in 5% CO for 24 h. After this period, the medium containing the test substance was aspirated from the wells and 10 µL of MTT solution (5 mg/ml) and 90 µL of fresh broth medium were added to each well to obtain a final concentration of 0.5 mg/ml MTT and then incubated for 4 hours at 37 °C. Optical density was read at 570 nm and 630 nm in the ELISA reader. Cell viability percentages were determined using the formula [(570 nm-630 $nm_{(test\ (compound\ applied)\ cell\ group)}$/(570 nm-630 $nm)_{(control\ (no\ compound\ applied)\ cell\ group)}$]x100. IC_{50} was calculated based on logarithmic cell viability percentages.

DPPH free radical scavenging activity

The study utilized DPPH (2,2-diphenyl-1-picrylhydrazyl) to investigate the free radical-scavenging activities of the compounds. To perform the analysis, 1 ml of the compounds was added to 1.0 ml of a methanolic solution containing 0.3 mM DPPH. The mixture was thoroughly shaken and then placed in a dark box at room temperature (30°C) for a duration of 30 minutes. Following this incubation period, the absorbance of the resulting solution was measured at 517 nm. The inhibitory percentage of DPPH was determined using the following equation:

$$\text{Scavenging activity} = \left[\left(\frac{\text{Control absorbance} - \text{sample absorbance)}}{\text{absorbance of control}}\right) \text{X } 100\%\right]$$

3. Results and Discussion

3.1- Preparation of the PEPPSI-Pd(II)–N-heterocyclic carbene (NHC) complex 3

The synthetic methodology used for both N-heterocyclic carbene precursors and palladium complexes is summarized in **Scheme 1**. The compounds were prepared according to our previous work.[57] N-heterocyclic carbene precursors were prepared in good yield (>75%) in a two-step N-alkylation process as shown in **Scheme 1**. At the first step, methyl group was introduced to the 5,6-dimethyl benzimidazole in THF at 60°C for 16h that enhancing the reactivity of the other the nitrogen atom. The addition of the other alkyl halides to the remaining nitrogen atom gave the desired N-heterocyclic carbene precursors **2a-i**. The solvent used for the reaction was DMF at 80°C for 3 days. These N-heterocyclic carbene precursors (NHC) were used for the synthesis of PEPPSI-type palladium complexes using a one-pot strategy developed by Organ and co-workers.[58] Palladium complexes **3a-i** were synthesized in the reaction of corresponding N-heterocyclic carbene precursor with $PdCl_2$ in the presence of K_2CO_3 in pyridine at 80°C for 5 h in good yield (>80%) using this methodology. All the ligand precursors and complexes were air, light, and moisture stable both in solution as well as in solid-state form. DCM: diethylether and DCM: npentane mixtures were used for the recrystallization of ligand precursors and complexes, respectively. Complex **3a** produced crystals suitable for single-crystal analysis.

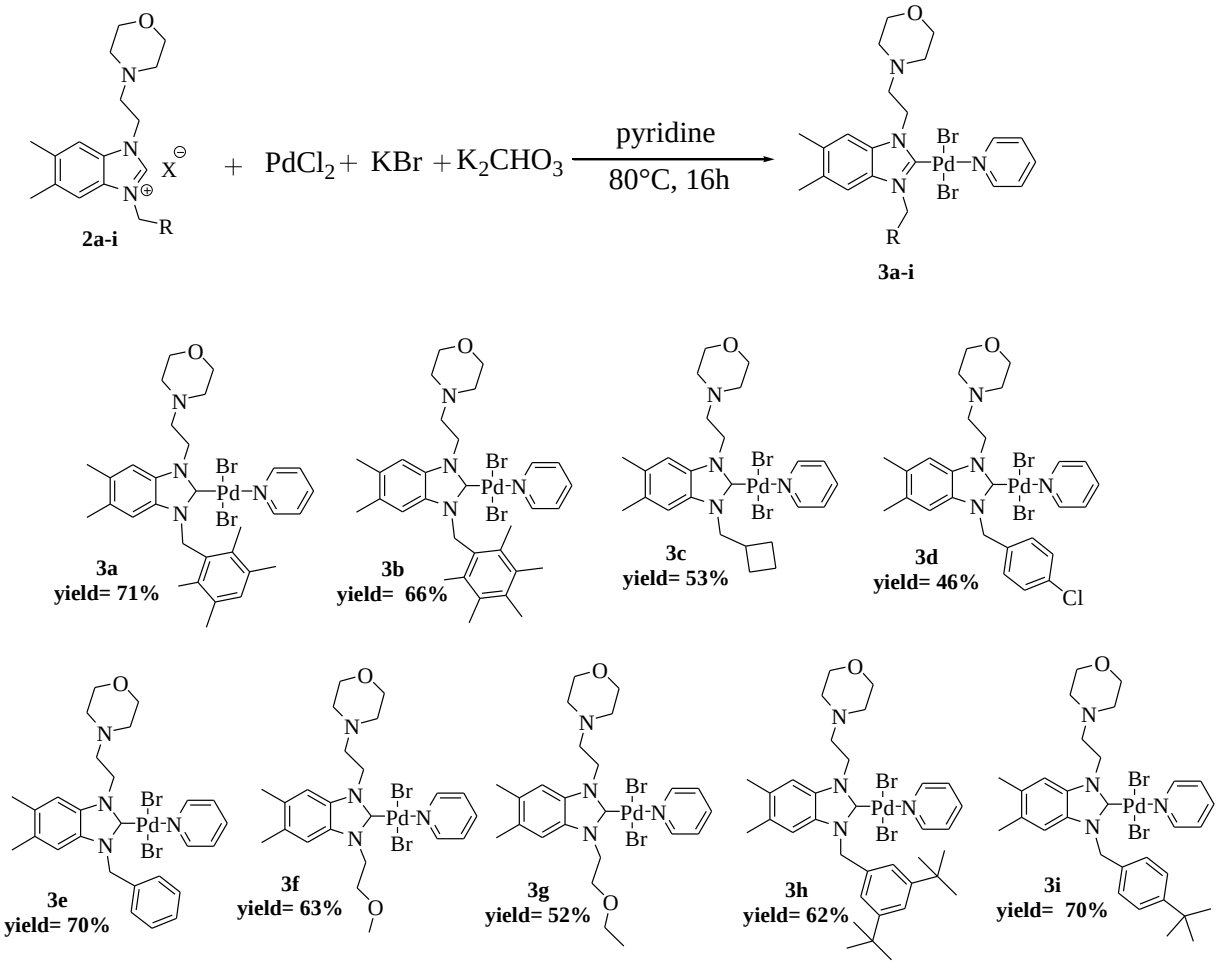

Scheme 1 : Synthesis of the PEPPSI- Pd- NHC complexes (**3a–i**)

The structures of all the synthesized compounds were fully characterized by NMR (^{1}H, ^{13}C{1 H}), FT-IR spectroscopy and elemental analysis. In the ^{1} HNMR ($CDCl_3$) spectra, NHC imino proton of N-heterocyclic carbene precursors were observed as a sharp singlet at chemical shifts of 11.83, 11.82, 11.66, 11.70 and 11.25 ppm, respectively, for **2a-i**. As evidence of complex formation, signals attributable to the NHC imino protons were absent from the ^{1}HNMR spectra of the palladium complexes (**3a-i**). The ^{13}CNMR ($CDCl_3$) spectra of 2a-i had signals at 143.0, 143.5, 143.4, 143.5 and 143.0 ppm assigned to the NHC imino carbon. The characteristic palladium carbene carbon peaks were seen at 162.3, 163.1, 163.0, 162.7 and 161.9 ppm for **3a-i**, respectively, in accordance with the literature. After complexation, NCN carbene resonance on the palladium complex shifted much downfield region compared to the corresponding N-heterocyclic carbene precursor which is another

indicator of complex formation. The signal of the benzylic proton (N-CH-Ar) belonging to palladium complexes (**3a-i**) gave signal as a sharp singlet signal at 6.17, 6.62, 6.27, 6.11 and 6.14 ppm, respectively. In the palladium complexes (**3a-i**), the α-protons peak of pyridine appeared at around 8.99–8.91 ppm. At the infrared spectra of the NHC precursors (**3a-i**), a specific υ(C=N) band was seen at 1554, 1557, 1555, 1558 and 1549 cm^{-1}. The complex were characterized by mass spectrometry, which show many peaks due to formation of various fragments. Although it is difficult to observe the molecular ion peak because this molecular ion break into fragments.

Crystal structure

The complex *trans*-[Pd(py)(L)Br_2] forms monoclinic crystals in space group *C*2/c and, as expected, the structure is built up from mononuclear units. Structural data for carbene PEPPSI-Pd(II)–N-heterocyclic carbene (NHC) complex are abundant, [59], but species derived from $PdBr_2$ are relatively rare, [60-61]. With only 2 entries [60] in the Cambridge Structural Database (CSD), being of those where both bromide anions are coordinated as in the present case. Thus, the Pd(II) coordination sphere (**Figure 1**) has a distorted square planar form, with Pd(1)-C(8) 1.957(4) Å, Pd(1)-N(6) 2.100(4) Å, Pd(1)-Br(2) 2.4471(7) Å and Pd(01)-Br(3) 2.4414(7) Å, and C(8)-Pd(1)-N(6) 179.1(2)°, Br(2)-Pd(1)-Br(3) 174.1(1)°, C(8)-Pd(1)-Br(2) 88.6(1)°, C(008)-Pd(1)-Br(3) 89.4(1)°, N(6)-Pd(1)-Br(2) 91.8(1)° and N(6)-Pd(1)-Br(3) 90.3(1)°. While the bond lengths between Pd and Br in this complex are similar to those found in other $PdBr_2(NHC)_2$ complexes, with values of 2.444(1), 2.438(1), and 2.4335(4) Å. However, the Pd-C (carbene) bond length is noticeably shorter in this species, measuring 2.012(4) and 2.039(7) Å. This difference is likely due to the presence of a relatively weak pyridine-N donor, which causes the bound C-atom to be trans to it. Interestingly, the Pd-C bond length closely resembles that observed in a true PEPPSI-Pd(II)–N-heterocyclic carbene (NHC) complex of $PdCl_2$, which measures 1.964(3) Å. The bulky carbene-N substituents effectively block the axial sites on Pd, without any significant agostic Pd...H interactions [59]. Molecular structure of PEPPSI-Pd(II)–N-heterocyclic carbene (NHC) complex **3a** with the atom-numbering scheme is depicted in **Fig. 1**, while key bond lengths and angles are listed in Table 2.

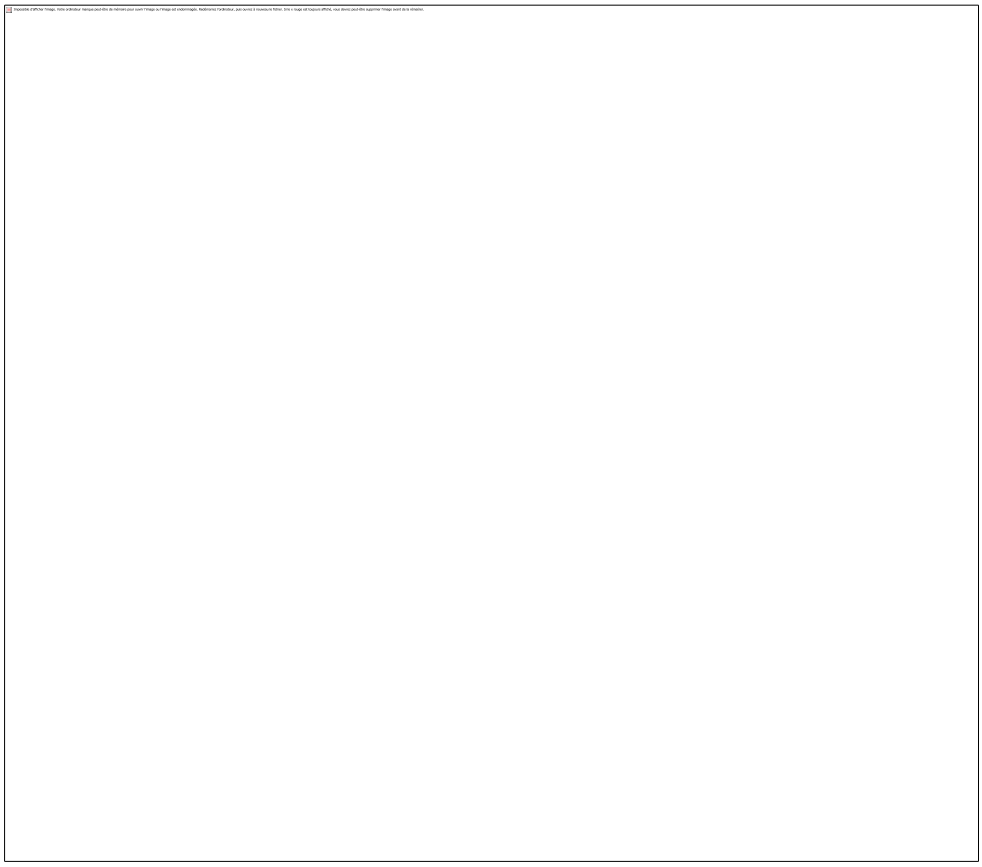

Figure 1. Molecular structure of PEPPSI-Pd(II)–N-heterocyclic carbene (NHC) complex **3a** showing the atom-numbering scheme.

The palladium atom is tetracoordinated to the carbene atom of the NHC, the nitrogen atom of the pyridine ring, and the two bromine atoms on the Br_2NC plane. The Pd(II) center exhibits a slightly distorted square planar geometry with PdBr2NC coordination, where the NHC and pyridine ligands, as well as the anionic atoms, are trans to each other. This distortion is observed as a deviation from linearity of the angle formed by Br─Pd─Br and N─Pd─C atoms, 174.13(3) and 179.12(17)°, respectively, as the *cis* angles vary from 88.58(14) to 91.82(12)°. The values of the four-coordinate indexes τ_4 [62] and τ_4' [63], which are 0 for an ideal square-planar geometry and 1 for an ideal tetrahedral coordination sphere, are 0.05 and 0.03, respectively, indicating a slightly distorted square-planar geometry. Table 2

Table 2. Selected geometric parameters for PEPPSI-Pd(II)–N-heterocyclic carbene (NHC) complex **3a**

Parameters		Parameters	
Bond lengths (Å)			
Pd1─Br1	2.4414(7)	N1─C1	1.358(5)
Pd1─Br2	2.4471(7)	N1─C2	1.394(5)
Pd1─N4	2.100(4)	N2─C1	1.361(5)
Pd1─C1	1.957(4)	N2─C9	1.407(5)
Bond angles (°)			
Br1─Pd1─Br2	174.13(3)	Br2─Pd1─C1	88.58(14)
Br1─Pd1─N4	90.29(12)	N4─Pd1─C1	179.12(17)
Br1─Pd1─C1	89.38(14)	N1─C1─N2	107.0(4)
Br2─Pd1─N4	91.82(12)		

The Pd─C bond distance [1.957(4) Å] is smaller than the sum of the individual covalent radii of the palladium and carbon atoms (2.12 Å), while the Pd─N bond distance [2.100(4) Å] is equal to the sum of the individual covalent radii of the palladium and nitrogen atoms (2.10 Å). The Pd─Br distances are in the usual range, and the internal N─C─N ring angle at the car- bene center is 107.0(4)°. Consequently, these parameters are comparable with those observed for analogous Pd-NHC-pyridine-Br_2 complexes [64-65]. The carbene ring is almost perpendicular to the coordination plane with a dihedral angle of 76.51(15)° as the dihedral angle between the pyridine ring and the coordination plane is 62.4(2)°. Furthermore, the benzene ring makes dihedral angles of 83.4(2) and 58.4(3)°, respectively, with the carbene and pyridine ring planes.

Hirshfeld surface analysis

Hirshfeld surface analysis provides a valuable way to visualize molecular interactions within a crystal. Using Crystal Explorer [66-67], these surfaces are computed for each molecule in a crystal, allowing for the identification of intermolecular contacts both on a molecular and overall structural level. By extending an atom's weight function to encompass its role in the crystal [68], Hirshfeld surfaces offer insights into interactions, particularly in crystals where hydrogen positions are precisely located [69]. Analysis of the 2D fingerprint plots (**Fig. 2**) for complex 3 indicates that the crystal structure is predominantly stabilized by hydrogen contacts—H…H interactions constitute about two-thirds of the overall interactions, while contributions from Br…H, C…H, O…H, and N…H contacts are also significant.

Furthermore, the Hirshfeld surface displayed in **Figure 3** highlights that, aside from dispersion forces, the only notable directional interaction is the Br…Br halogen bond (Br(02)…Br(03) at 3.6607(8) Å), which forms extended columns of complex units along the [001] axis. This arrangement suggests that the coordinated bromide might serve as an acceptor for nucleophilic donors during interactions with biomolecules. However, given the lability of Pd(II)-Br bonds in aqueous media, nucleophilic substitution at the metal center is a more likely pathway for reactivity.

In summary, the crystal packing of complex **3a** (crystallizing in the monoclinic space group C2/c) is maintained by a network of intermolecular forces where dispersion interactions, especially H…H contacts, play a major role. The specific Br…Br halogen bonds not only reinforce the stability of the crystal but also hint at potential reactivity via nucleophilic substitution at the Pd(II) center, which could be relevant to its biological activity.

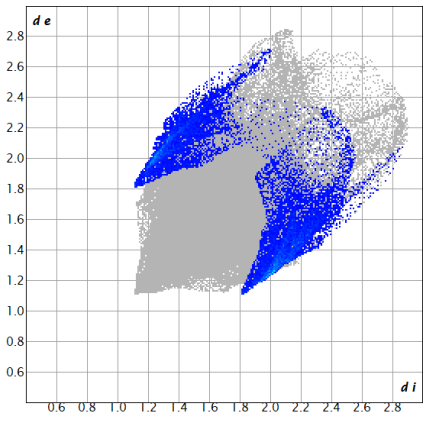

Br..H/H..Br 9.8%

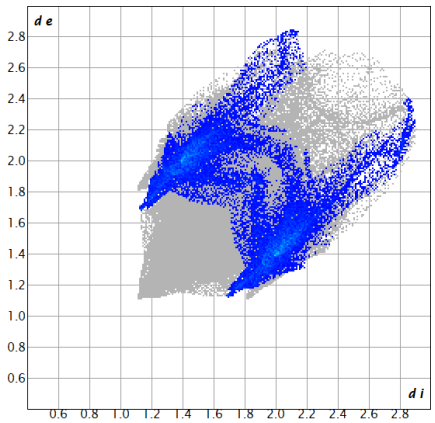

C..H/H..C 16.7%

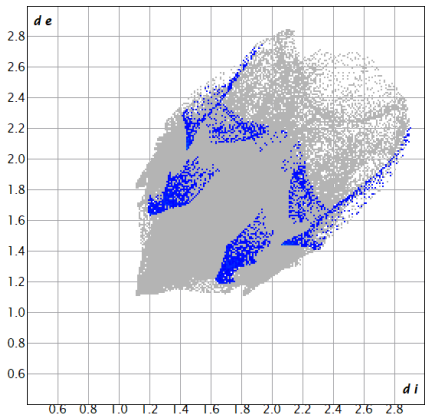

N..H/H..N 2.2%

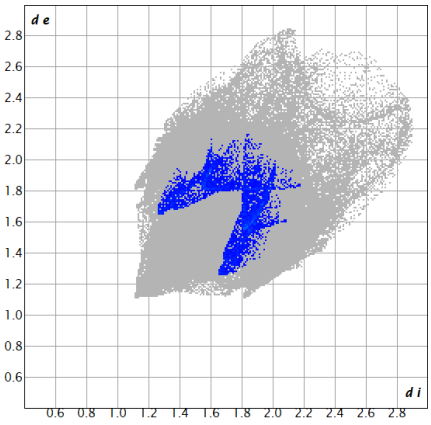

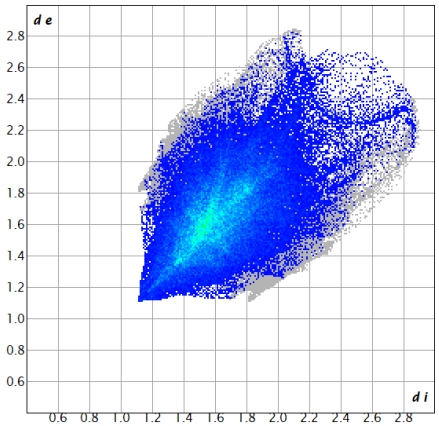

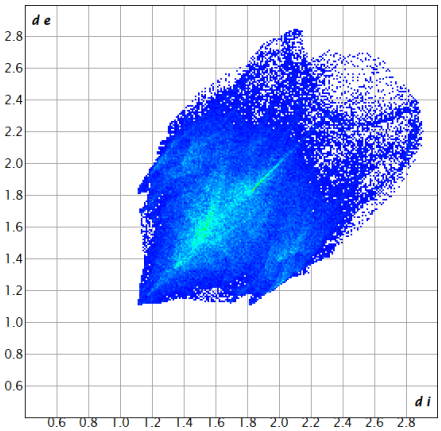

O..H/H..O 3.6% **H..H/H..H 66.0%** **All interactions 100%**

Figure 2: 2D Fingerprint plots of PEPPSI-Pd(II)–N-heterocyclic carbene (NHC) complex **3a**

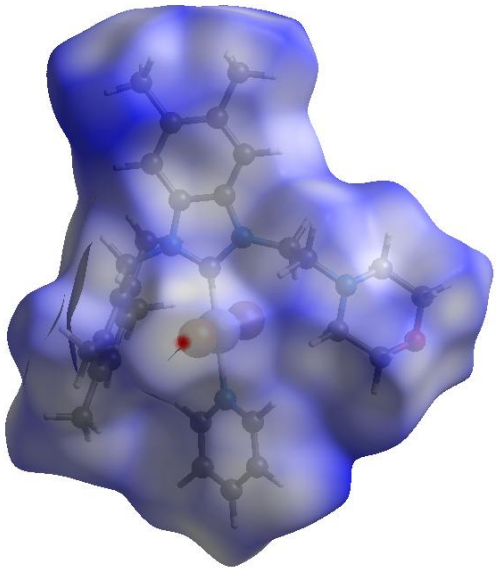

Figure 3: The Hirshfeld surface of PEPPSI-Pd(II)–N-heterocyclic carbene (NHC) complex **3a**, mapped with d_{norm}. The red regions adjacent to the bromo-ligands are the only points where interactions exceed dispersion.

DFT analysis

The structural and electronic properties of PEPPSI-Pd(II)-N-heterocyclic carbene (NHC) complexes (denoted as 3a-i) were investigated using Density Functional Theory (DFT) [70-71] to optimize their geometries and elucidate their electronic characteristics. The computations were performed with the B3LYP functional [72-74] and a mixed basis set: LANL2DZ for the palladium atom [75-76] and 6-311G++(2d,2p) for all other atoms, as implemented in Gaussian 16 software [77]. All optimized geometries correspond to local minima on the potential energy surface, with no imaginary frequencies observed. This confirms that the structures obtained are stable and represent true minima.

This computational approach provides a robust framework for examining the molecular properties of these complexes, offering insights into their potential reactivity and applications.

Structural Analysis

The optimized geometry of complex **3a**, shown in **Figure 4**, aligns well with the experimental crystallographic data obtained from X-ray diffraction (XRD), as detailed in Table 3. This table lists key geometric parameters, including bond lengths (in Å) and bond angles (in °), for

the series of complexes alongside the experimental values. For instance, the Pd1-Br1 bond length is experimentally determined as 2.4414(7) Å, while the calculated values range from 2.520 Å to 2.524 Å across complexes **3a-i**. Similarly, the Pd1-C1 bond, associated with the NHC ligand, is experimentally 1.957(4) Å and computed between 1.980 Å and 1.983 Å. Despite a slight overestimation in bond lengths, which is typical for DFT calculations using the LANL2DZ basis set due to its effective core potential approximation, the computational model demonstrates good accuracy, with RMSD values of 0.0493 Å for bond lengths and 1.6745° for angles in complex 3a, thereby confirming its reliability.

The inclusion of Root Mean Square Deviation (RMSD) values provides a quantitative measure of the agreement between the computed and experimental structures. Specifically, an RMSD of 0.0493 Å for bond lengths and 1.6745° for angles in complex 3a indicates that the deviations are minimal and within acceptable limits for such computational methods, reinforcing the trustworthiness of the model for structural analysis.

Electronic Properties

The calculated HOMO-LUMO energy gap for complex **3** is 3.55 eV, a value characteristic of semiconductor-like materials. This moderate band gap implies sufficient electronic stability while allowing for potential electron transfer processes, which could be advantageous in applications such as bio-sensing or catalysis.

The DFT analysis of PEPPSI-Pd(II)-NHC complexes **3a-i** reveals a robust computational model that accurately reproduces experimental geometries and provides valuable electronic insights. The close alignment of bond lengths and angles with experimental data, as shown in Table 3, validates the use of the B3LYP/LANL2DZ:6-311G++(2d,2p) method. The electronic structure, with a 3.55 eV band gap and distinct HOMO-LUMO localization, suggests potential reactivity profiles that could be exploited in biological or catalytic contexts. Table 4 These findings lay a foundation for future studies, such as exploring substituent effects on the electronic properties or experimental validation of the predicted interaction sites.

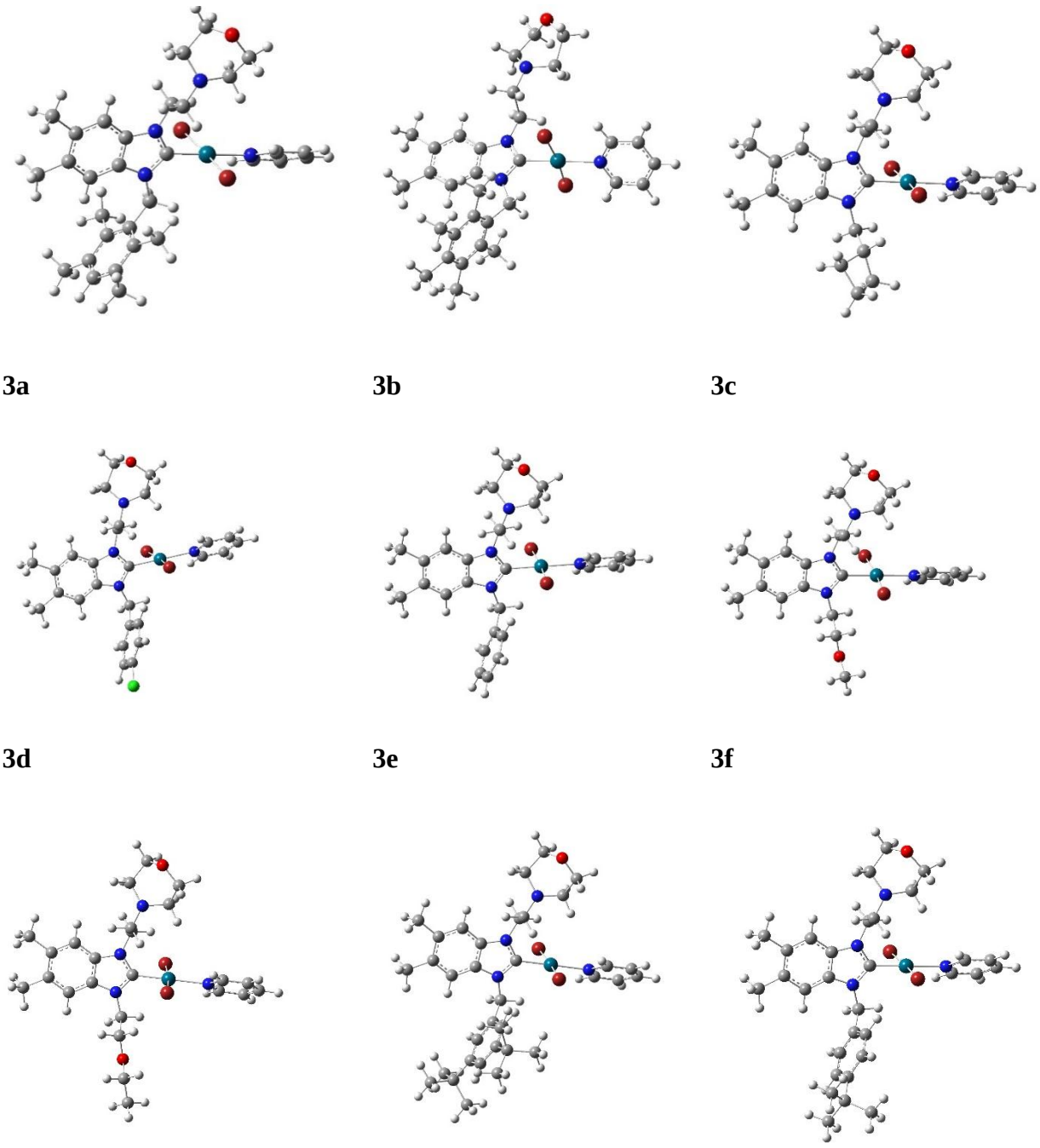

Figure 4: Optimized structure for PEPPSI-Pd(II)–N-heterocyclic carbene (NHC) complexes **3a-i** at DFT B3LYP/6-311G++(2d, 2p): LANL2DZ level of theory

Table 3: Computed geometric parameters of PEPPSI-Pd(II)–N-heterocyclic carbene (NHC) complexes **3a-i at DFT B3LYP/6-311G++(2d, 2p): LANL2DZ level of theory**

Geometric parameter	XRD	3a	3b	3c	3d	3e	3f	3g	3h	3i
Bond length in (Å)										
Pd1-Br1	2.4414(7)	2.520	2.522	2.523	2.522	2.522	2.523	2.523	2.524	2.523
Pd1-Br2	2.4471(7)	2.520	2.520	2.517	2.516	2.517	2.515	2.516	2.516	2.517
Pd1-N4	2.100(4)	2.184	2.187	2.185	2.181	2.181	2.181	2.182	2.182	2.182
Pd1-C1	1.957(4)	1.983	1.980	1.982	1.983	1.983	1.981	1.981	1.983	1.983
N1-C1	1.358(5)	1.348	1.347	1.351	1.349	1.350	1.350	1.350	1.350	1.350
N1-C2	1.394(5)	1.392	1.392	1.393	1.395	1.395	1.395	1.394	1.395	1.395
N2-C1	1.361(5)	1.351	1.351	1.351	1.353	1.352	1.352	1.352	1.352	1.352
N2-C9	1.407(5)	1.402	1.402	1.394	1.395	1.395	1.394	1.394	1.395	1.395
RMSD	-	0.0493	0.0502	0.0496	0.0484	0.0486	0.0484	0.0488	0.0491	0.0490
Angles in (°)										
Br1-Pd1-Br2	174.13(3)	174.1	173.3	174.1	174.1	174.3	174.0	173.9	174.3	174.2
Br1-Pd1-N4	90.29(12)	92.8	93.2	92.7	92.7	92.7	92.8	93.1	92.6	92.7
Br1-Pd1-C1	89.38(14)	88.6	87.5	88.4	88.4	88.5	88.1	88.1	88.6	88.5
Br2-Pd1-N4	91.82(12)	93.1	93.5	93.1	93.1	93.0	93.1	92.9	92.9	93.0
Br2-Pd1-C1	88.58(14)	85.5	85.8	85.8	85.7	85.8	86.0	86.0	85.8	85.8
N4-Pd1-C1	179.12(17)	178.5	179.1	178.8	178.7	178.7	178.8	178.8	178.6	178.7
N1-C1-N2	107.0(4)	108.1	108.2	107.7	107.6	107.6	107.6	107.6	107.7	107.6
RMSD	-	1.6745	1.8777	1.5460	1.5693	1.5245	1.5452	1.5979	1.4942	1.5234

Table 4: Computed HOMO, LUMO energy levels and energy gap (in eV) of peppsi-pd(ii)–n-heterocyclic carbene (nhc) complexes **3a-i** using dft b3lyp/6-311++g(2d,2p) with lanl2dz level of theory

Complex	ε_{LUMO}	ε_{HOMO}	Energy gap
3a	-2.01	-5.73	3.72
3b	-1.97	-5.72	3.75
3c	-2.03	-5.75	3.72
3d	-2.15	-5.82	3.67
3e	-2.07	-5.76	3.69
3f	-2.05	-5.79	3.74
3g	-2.04	-5.78	3.74

3h	-2.06	-5.75	3.70
3i	-2.05	-5.75	3.70

Charge transfer CT analysis

The Charge Transfer (CT) analysis of the PEPPSI-Pd(II)-N-heterocyclic carbene (NHC) complexes **3a-i** elucidates a sophisticated intramolecular electronic interplay, as delineated by **Figure 5** and quantified in Table 5. Fragment 1, presumably the NHC ligand, exhibits a persistent positive charge (e.g., +0.53296 to +0.55183 e), indicative of substantial σ-donation to Fragment 2 (likely the $PdBr_2$ moiety), which consistently bears a negative charge (-0.72905 to -0.75312 e), reflecting its role as an electron sink stabilized by the palladium d-orbitals and bromine p-orbitals. Fragment 3, with a modest positive charge (+0.19505 to +0.21592 e), appears to fine-tune this charge polarization, potentially via π-backbonding or inductive effects from the pyridine or substituent groups inherent to the PEPPSI framework. These charge distributions, derived from DFT computations, reveal a nuanced donor-acceptor dynamic that underpins the complexes' electronic asymmetry, with minimal variation across the series suggesting robust structural conservation despite substituent modulation. This electronic configuration enhances the electrophilicity of the palladium center, priming it for nucleophilic interactions critical in advanced catalytic applications (e.g., cross-coupling) and potentially influencing redox properties or biomolecular binding affinities, where the charge-localized $PdBr_2$ fragment could engage electron-rich biological targets, warranting further computational and experimental exploration to correlate these charge profiles with specific reactivity metrics.

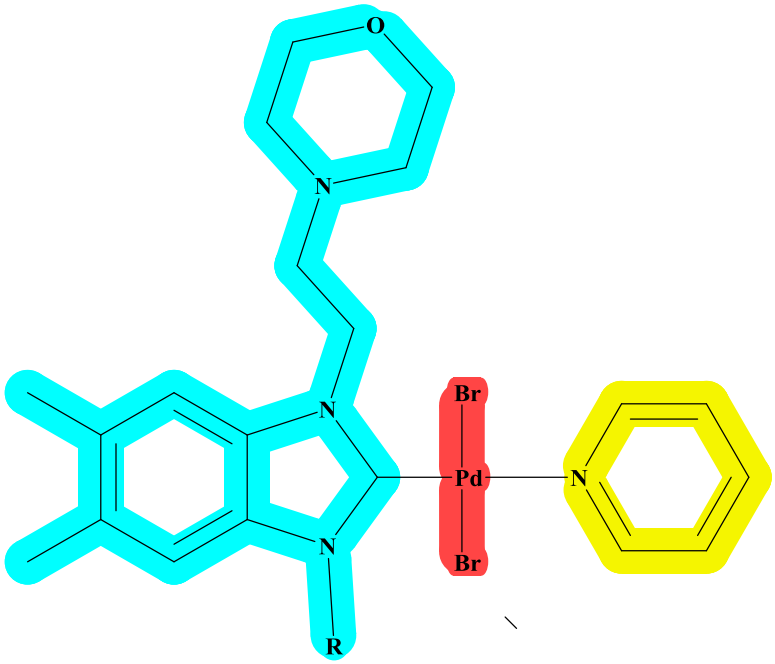

Figure 5: Three Fragments considered for 3a-i complexes (Blue: Fragment 1, Red: Fragment 2, Yellow: Fragment 3)

Table 5: Computed total charge (in Electrons) for each fragment in **3a-i** Pd-NHC complexes

Complex	Q1	Q2	Q3
3a	0.53769	-0.73092	0.19941
3b	0.54503	-0.73087	0.19648
3c	0.53956	-0.75312	0.21372
3d	0.54239	-0.75163	0.21592
3e	0.53740	-0.75132	0.21489
3f	0.53296	-0.74726	0.21541
3g	0.53429	-0.72905	0.19505
3h	0.55183	-0.75161	0.21433
3i	0.54543	-0.75296	0.21416

Anticancer (MTT) Test

In this study, the anticancer activity of **2a, 2b, 2c, 2d, 2e, 2f, 2g, 2h** and **2i** salts was evaluated on three different cell lines: BEAS-2B, a human healthy lung cell line; HCT116, a human colon cancer cell line; and SH-SY5Y, a human brain cancer cell line. Cisplatin was used as control group. The IC_{50} values calculated for cisplatin were 103.26±3.26 for BEAS-2B, 254.78±6.11 for HCT116 and 129.86±4.91 for SH-SY5Y, respectively. These reference values were used as criteria for the evaluation of the performance of the salts. Table 6

Table 6: Anticancer activities of salts 2 against different cell lines

IC_{50} (μM)					
ORDER NO	PLATE NO	CODE	BEAS2B	SHSY5Y	HCT116
1	**1**	**2a**	488,65±6,88	NA	44,77±3,99
2	**2**	**2b**	83,36±9,47	NA	30,43±8,27
4	**4**	**2c**	712,19±9,20	NA	51,62±0,27
5	**5**	**2d**	610,45±11,58	NA	48,45±0,74
6	**6**	**2e**	499,74±18,15	NA	337,01±91,74
7	**7**	**2f**	NA	NA	NA
8	**8**	**2g**	NA	NA	NA
9	**9**	**2h**	9,99±0,22	NA	9,26±1,53
10	**10**	**2i**	44,52±2,80	NA	33,03±2,17
	CISPLATIN		**103.26±3.26**	**129.86±4.91**	**254.78±6.11**

IC_{50} values presented as mean ± SD of three independent experiments.
NA: Not Applicable (IC_{50}>800 μM),

Among the tested salt, **2c** showed the lowest cytotoxicity with an IC_{50} value of 712.19±9.20, indicating minimal effect on healthy cells. In contrast, 2h exhibited the highest cytotoxicity with an IC_{50} value of 9.99±0.22. Salts such as **2a, 2d** and **2e** showed lower cytotoxicity compared to cisplatin. Furthermore, the salts **2f** and **2g** did not show cytotoxicity. In contrast, **2h** exhibited the highest cytotoxicity with an IC_{50} value of 9.99±0.22. Salts such as **2a, 2d** and **2e** showed lower cytotoxicity compared to cisplatin. In addition, **2f** and **2g** salt did not show cytotoxicity on this cell line.

When IC_{50} values on HCT116 Colon Cancer Cells were analysed, **2e** showed the lowest cytotoxicity with an IC_{50} value of 337.01±91.74. The highest cytotoxicity was observed in 2h with an IC_{50} value of 9.26±1.53. Salts **2a, 2b, 2c, 2d, 2h** and **2i** showed higher cytotoxicity compared to cisplatin. In contrast, **2f** and **2g** salts did not show cytotoxicity in this cell line.

For SH-SY5Y brain cancer cell line, the control drug cisplatin with IC_{50} value of 129.86±4.91 exhibited the highest cytotoxicity among all compounds tested. All other salt complexes showed no cytotoxic effect when IC_{50} values were analysed.

2a exhibited low cytotoxicity with an IC_{50} value of 488.65±6.88 in the healthy cell line BEAS-2B. It showed high cytotoxicity against the colon cancer cell line HCT116 with an IC_{50} value of 44.77±3.99, while it did not show cytotoxicity against the brain cancer cell line SH-SY5Y. These results suggest that **2a** can effectively target colon cancer cells while protecting healthy lung cells.

2b showed low cytotoxicity with an IC_{50} value of 83.36±9.47 in BEAS-2B and high cytotoxicity with an IC50 value of 30.43±8.27 in HCT116. It did not exhibit cytotoxicity against SH-SY5Y.

2h exhibited high cytotoxicity in both BEAS-2B and HCT116. The IC_{50} value for BEAS-2B was 9.99±0.22 and 9.26±1.53 for HCT116. However, it was not toxic for SH-SY5Y. Despite its activity against colon cancer cells, it showed significant toxicity against healthy lung cells.

In this study, complexes that showed low cytotoxicity in the healthy cell line BEAS-2B but high cytotoxicity in the cancer cell lines HCT116 and SH-SY5Y were considered to have potential anticancer properties. On the other hand, **2h** was the most effective complex against the colon cancer cell line HCT116 with an IC_{50}value of 9.26±1.53. However, its high toxicity in the healthy cell line BEAS-2B with an IC_{50} value of 9.99±0.22 suggests that it requires further optimisation to increase its selectivity.

These findings highlight the potential of various complexes for future drug development, especially those that show selective cytotoxicity against cancer cells while sparing healthy tissues.

The anticancer properties of Pd-NHC complexes **3a-i** were investigated on three different cell lines, namely BEAS-2B (human healthy lung cell), HCT116 (human colon cancer) and SH-SY5Y (human brain cancer). The IC_{50} values of cisplatin used as control group on these cell lines were calculated as 103.26 ± 3.26, 254.78 ± 6.11 and 129.86 ± 4.91, respectively. Table 7

Complex **3g** showed the lowest cytotoxicity in BEAS-2B cell line. The IC_{50} value of this complex was 218.46 ± 4.24, indicating low cytotoxicity in healthy cell line. 3a and 3h also showed low cytotoxic effect with IC_{50} values of 332.78 ± 12.61 and 333.82 ± 20.09, respectively. 3f showed the highest cytotoxicity and IC50 value was measured as 430.09 ± 45.76. Apart from this, **3b, 3c, 3d** complexes did not show cytotoxicity against BEAS-2B cell line.

Table 7 : Anticancer activities of Pd-NHC complexes **3a-i** against different cell lines

			IC_{50} (μM)		
ORDER NO	PLATE NO	CODE	BEAS2B	SHSY5Y	HCT116
21	**21**	**3a**	332,78±12,61	NA	403,98±8,39
22	**22**	**3b**	NA	NA	281,36±3,56
23	**23**	**3c**	NA	NA	NA

24	**24**	**3d**	NA	NA	NA
25	**25**	**3e**	NA	561,90±48,10	NA
26	**26**	**3f**	430,09±45,76	595,74±88,49	311,01±22,02
27	**27**	**3g**	218,46±4,24	349,71±30,04	204,96±15,65
28	**28**	**3h**	333,82±20,09	637,05±24,77	217,07±2,73
29	**29**	**3i**	400,96±42,98	NA	265,29±5,13
	CISPLATIN		**103.26±3.26**	**129.86±4.91**	**254.78±6.11**

IC_{50} values presented as mean ± SD of three independent experiments.
NA: Not Applicable (IC_{50}>800 µM),

Complex **3g** showed the highest cytotoxicity in HCT116 cell line. IC_{50} value was 204.96 ± 15.65 and this complex was more effective than Cisplatin. **3g** and **3a** also showed cytotoxic effect with IC_{50} values of 265.29 ± 5.13 and 403.98 ± 8.39, respectively. However, **3b** and **3d** did not show cytotoxicity against this cell line.

3g showed the highest cytotoxicity in SH-SY5Y cell line. IC_{50} value of this complex was 349.71 ± 30.04 and it was determined that this complex showed lower cytotoxic effect compared to Cisplatin. The lowest cytotoxicity was shown by **3h** and IC_{50} value was measured as 637.05 ± 24.77. **3a**, **3b**, **3c**, **3d** and **3a** did not show cytotoxicity against this cell line. **3g** showed the highest cytotoxicity in both HCT116 and SH-SY5Y cell lines. The high IC_{50} value in the healthy cell line indicates that this complex shows high cytotoxic effect in cancerous cell lines but has lower toxicity in healthy cells. **3f** showed the lowest toxicity in the healthy cell line. However, it showed a moderate cytotoxic effect in HCT116 cell line. In addition, it did not show an effective cytotoxicity in SH-SY5Y cell line. **3b** had an IC_{50} value of NA in all cell lines and showed no cytotoxic effect against any cell line.Within the scope of the study, complexes with low toxicity in healthy cell lines and high toxicity in cancer cell lines can be considered as promising candidates for anticancer drug development studies. Especially **3g** stands out as a potential anticancer agent by showing high cytotoxic effect in both cancerous cell lines. In addition, **3f,** which shows low toxicity in healthy cell lines, is also among the complexes to be evaluated.

Antioxidant activities of salts 2 and their complexes 3

The antioxidant capacity of the produced compounds was assessed using DPPH assays and compared to a positive control, Butylated hydroxytoluene (BHT) (50 ug/ml). Table 8 presents the results, indicating that compound **3d** demonstrated a significant outcome (38.19±0.33, 14.37±0.4, and 0.0) at concentrations of 2.0, 1.0, and 0.5 mg/mL, respectively. Similarly, the

DPPH activity of compounds **3a**, **3b**, and **3c** exhibited a gradual increase, ranging from 05.87±0.2, 11.87±0.1, and 08.87±0.4% at a concentration of 1.0 mg/mL to 33.21±2.1, 36.21±0.12, and 35.87±0.22% at a concentration of 2.0 mg/mL, respectively. On the other hand, all compounds showed no antioxidant activities with DPPH activity at concentrations 0.5 mg/mL. Moreover, compounds (**2a**, **2b**, **2c**, **2d**, and **2e**) showed only DPPH activity at concentrations 2.0 $mg.mL^{-1}$ with scavenging activity 20.24±0.2, 22.22±0.1, 23.41±0.2, 26.52±0.8 and 24.44±0.9, respectively. Table 9 The redox properties of these compounds, which allow them to behave as reducing agents or hydrogen atom donors while also scavenging free radicals, may account for their antioxidant activity. The DPPH odd electron can be partnered with a hydrogen atom or donated electrons. The results reveal that the phenyl ring substituents relate to the synthesized compounds potential antioxidant activity. The results obtained is similar either with our recent publication which reported antioxidant capacity of Pd complexes using DPPH method [78].

Table 8. Scavenging activity of synthesized compounds

No	**code**	**Antioxidant Activity**		
		DPPH%		
		2.0 $mg.mL^{-1}$	1.0 $mg.mL^{-1}$	0.5 $mg.mL^{-1}$
1	**Control (BHT)**	93.61 ± 2.8	75.60 ± 1.8	58.80 ± 1.8
2	**2a**	20.24 ± 0.2	0.0	0.0
3	**2b**	22.22 ± 0.1	0.0	0.0
4	**2c**	23.41 ± 0.2	0.0	0.0
5	**2d**	26.52 ± 0.8	0.0	0.0
6	**2e**	24.44 ± 0.9	0.0	0.0
7	**2f**	24.21 ± 0.1	0.0	0.0
8	**2g**	22.31 ± 0.2	0.0	0.0
9	**2h**	25.42 ± 0.8	0.0	0.0
10	**2i**	23.34 ± 0.9	0.0	0.0
11	**3a**	32.21 ±.2.1	05.87 ± 0.2	0.0
12	**3b**	35.21 ± 0.12	11.87 ± 0.1	0.0
13	**3c**	34.87 ± 0.22	08.87± 0.4	0.0
14	**3d**	37.19 ± 0.33	14.37 ± 0.4	0.0
15	**3e**	33.25 ± 0.32	15.28 ± 0.4	0.0

16	**3f**	32.11 ± 0.12	12.86 ± 0.1	0.0
17	**3g**	33.85 ± 0.22	08.76 ± 0.4	0.0
18	**3h**	35.18 ± 0.33	14.36 ± 0.4	0.0
19	**3i**	31.24 ± 0.32	15.25 ± 0.4	0.0
* The experiment was carried out in triplicate. Values are given as mean ± standard error. * Butylated hydroxytoluene (BHT)				

Table 9. IC_{50} values of antioxidant activities, DPPH and ABTS radical scavenging a of compounds **2a–e** and **3a-e** .

IC_{50} (µg mL^{-1}) / Compounds	DPPH	ABTS
2a	56.27	39.12
2b	61.45	36.14
2c	43.23	31.27
2d	62.25	52.21
2e	44.1	40.1
2f	59.34	32.13
2g	41.12	31.27
2h	58.23	52.21
2i	40.2	40.1
3a	60.4	42.78
3b	54.12	34.05
3c	61.38	47.04
3d	70.4	19.17
3e	65.2	83.2
3f	59.3	23.04
3g	52.21	36.03
3h	60.27	18.18
3i	71.3	84.1
BHT	85.2	84.5

ADMET study

The ADMET analysis of the PEPPSI-Pd(II)-NHC complexes 3a-i, conducted via ADMETlab 3.0, was performed by analyzing both **Fig. 6** and **the supporting information**. This comprehensive evaluation provides insights into their pharmacokinetic and toxicological properties, crucial for assessing their potential as drug candidates. This study encompasses nine complexes, with their multidimensional properties visualized in **Figure 6** through radar plots, revealing both uniform trends and subtle variations that inform their drug development prospects. A key clarification emerges regarding molecular weights: the reported range of 405.28–419.29 Da likely reflects the salt forms of these complexes (e.g., including

counterions such as bromide), not necessarily the neutral Pd-NHC entities, impacting the interpretation of physicochemical and pharmacokinetic data.

Physicochemical and Medicinal Chemistry Insights

The physicochemical properties, as depicted in **Figure 6**, indicate that the salt forms of complexes **3a-i** possess molecular weights (405.28–419.29 Da) within the 100–600 Da drug-likeness range, though exceeding the GSK Rule's 400 Da cutoff, hinting at potential ADMET challenges. The Topological Polar Surface Area (TPSA) remains a consistent 18.95 $Å^2$, well below 140 $Å^2$, suggesting excellent cell permeability, a feature visually compact in the radar plots' TPSA segments. However, high lipophilicity (log P): 4.869–5.069; (log D): 3.827–4.175) breaches the Pfizer Rule, flagging toxicity risks amplified by the expansive lipophilicity arcs in Figure 7. Solubility (log S): -5.611 to -5.171) suggests moderate aqueous solubility, potentially limiting bioavailability, a constraint evident in the plots' solubility profiles. Flexibility (0.227–0.273), with 5–6 rotatable bonds, supports conformational adaptability, while Quantitative Estimate of Drug-likeness (QED: 0.679–0.718) and synthetic accessibility (3.0) affirm pharmaceutical feasibility. Despite violating GSK and Golden Triangle Rules, adherence to Lipinski's Rule and the absence of PAINS or BMS alerts indicate a promising scaffold, though the salt-specific molecular weights suggest counterion effects may need consideration in optimization.

Absorption and Distribution Dynamics

Absorption properties, vital for bioavailability, present a mixed outlook, visually synthesized in Figure 7. Caco-2 permeability (-5.084 to -4.944) exceeds the -5.15 threshold, indicating moderate to good intestinal absorption, yet low MDCK and PAMPA values suggest passive diffusion limitations, reflected in the radar plots' inward absorption segments. High P-glycoprotein (Pgp) inhibition (0.881–0.997) and substrate probabilities (0.847–0.993) signal efflux barriers, with 3a and 3b showing slightly superior Caco-2 values (-5.084, -5.067). Distribution properties reveal high Plasma Protein Binding (PPB: 95.712%–97.117%), exceeding <90%, reducing free fractions (Fu: 2.893%–3.914%), as seen in Figure 7's pronounced PPB spokes. Volume of Distribution (VDss: 0.334–0.479 L/kg) is favorable, but Blood-Brain Barrier (BBB) penetration varies—high for 3a and 3b (0.984–0.999), low for 3c and 3d (0.005–0.006)—suggesting tailored CNS potential, a distinction clear in the plots' BBB profiles.

Metabolism and Excretion Profiles

Metabolism properties highlight drug-drug interaction risks and stability variations, as illustrated in Figure 6. CYP1A2 inhibition (0.939–0.962, except **3c** at 0.023) and CYP3A4 (0.836–0.995) are notably high, posing interaction concerns, while CYP2C9 and CYP2D6 show lower risks. Human Liver Microsomal (HLM) stability diverges, with 3a and 3b stable (>30 min) versus 3c and 3d unstable (≤30 min), a contrast visible in the radar plots' stability arcs. Excretion exhibits moderate clearance (7.845–8.59 mL/min/kg) but ultra-short half-lives (0.127–0.254 h), a limitation emphasized by Figure 6's compact half-life segments, necessitating strategies to extend duration.

Toxicity Considerations

Toxicity profiles, critical for safety, present significant hurdles, prominently displayed in Figure 6. High hERG blockade (0.557–0.925) and Drug-Induced Liver Injury (DILI: 0.901–0.967) probabilities indicate cardiotoxicity and hepatotoxicity risks, mirrored by extended toxicity spokes. AMES mutagenicity varies (0.426–0.86, lowest in **3c**), with additional concerns for skin sensitization and neurotoxicity, though rat oral acute toxicity remains moderate (0.331–0.488). Environmental impact is least for **3i**, a nuance captured in Figure 7's narrower environmental toxicity segment.

Implications for Drug Development

Integrated with Figure 6, this ADMET analysis positions **3c, 3d, 3e**, and **3f** as balanced candidates due to moderate absorption, improved distribution, and lower mutagenicity, though their high DILI and short half-lives demand attention. Complexes 3a and 3b excel in CNS penetration but face toxicity challenges, while **3g** and **3h** offer safer profiles yet struggle with absorption, trends visually synthesized in the radar plots. The salt-specific molecular weights suggest counterion contributions (e.g., Br^-) that may elevate (log P) and PPB, necessitating structural tweaks—such as reducing lipophilicity or modifying ionic interactions—to enhance solubility and safety. Sustained-release formulations could address the rapid excretion, leveraging the complexes' synthetic feasibility for optimization. This comprehensive profiling, visually reinforced by Figure 6, underscores the need for targeted refinements to unlock their therapeutic potential.

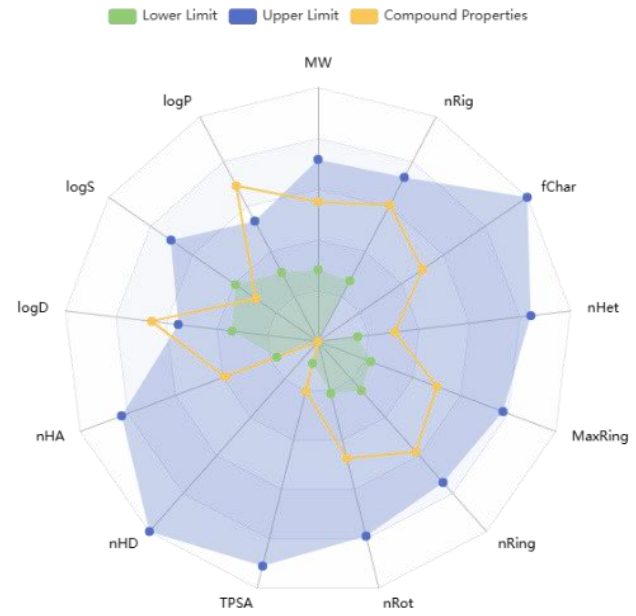
Lower Limit
Upper Limit
Compound Properties
MW
nRig
fChar
nHet
MaxRing
nRing
nRot
TPSA
nHD
nHA
logD
logS
logP

3a

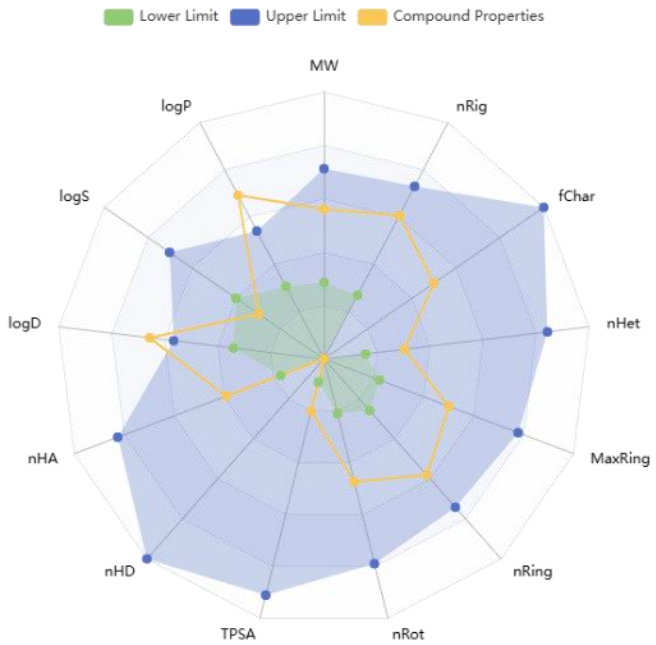
Lower Limit
Upper Limit
Compound Properties
MW
nRig
fChar
nHet
MaxRing
nRing
nRot
TPSA
nHD
nHA
logD
logS
logP

3b

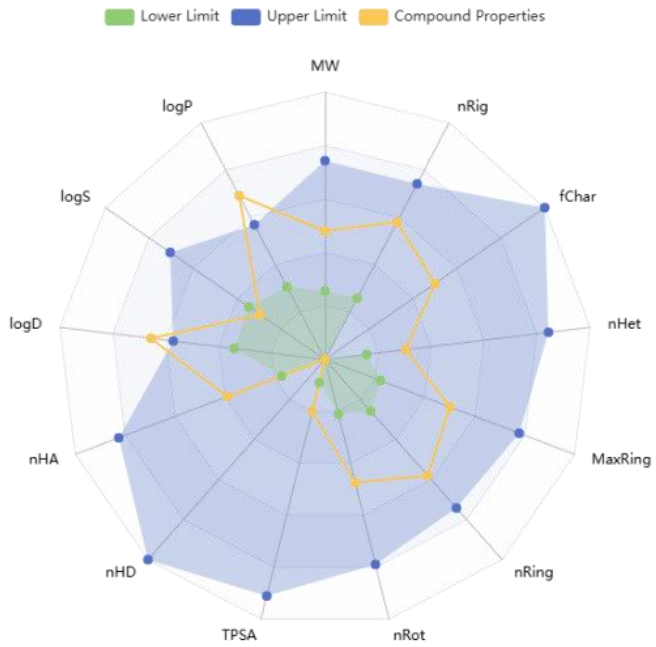
Lower Limit
Upper Limit
Compound Properties
MW
nRig
fChar
nHet
MaxRing
nRing
nRot
TPSA
nHD
nHA
logD
logS
logP

3c

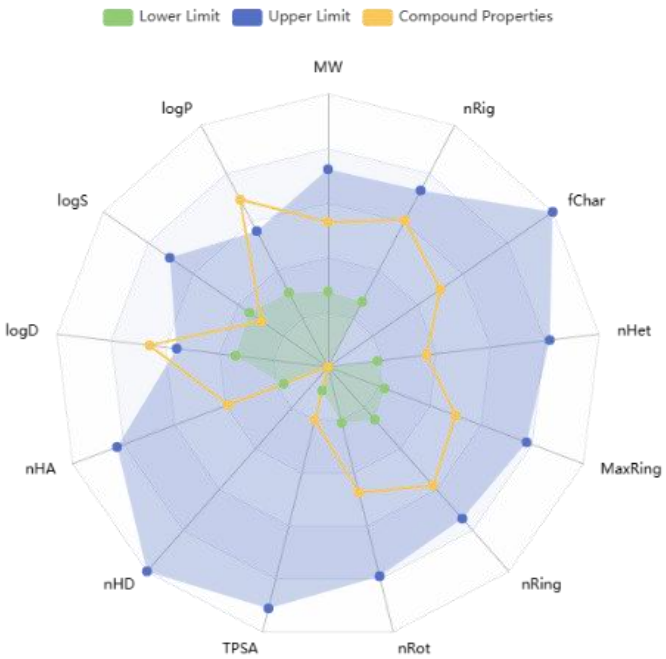
Lower Limit
Upper Limit
Compound Properties
MW
nRig
fChar
nHet
MaxRing
nRing
nRot
TPSA
nHD
nHA
logD
logS
logP

3d

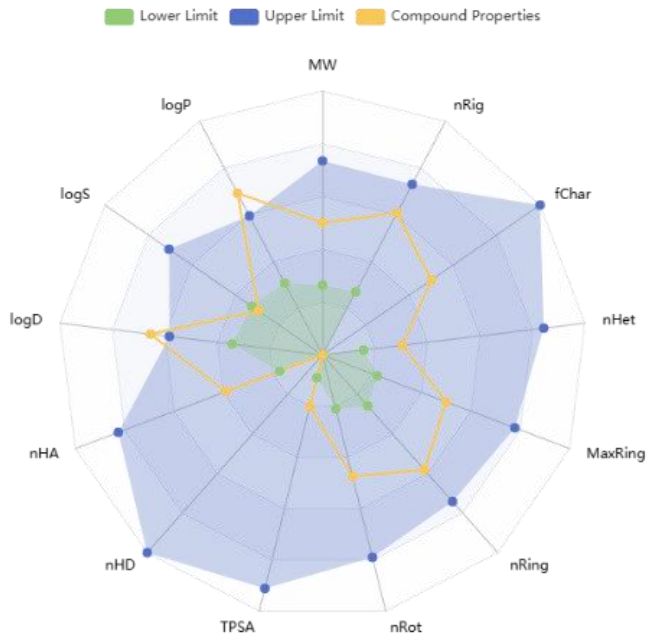
Lower Limit
Upper Limit
Compound Properties
MW
nRig
fChar
nHet
MaxRing
nRing
nRot
TPSA
nHD
nHA
logD
logS
logP

3e

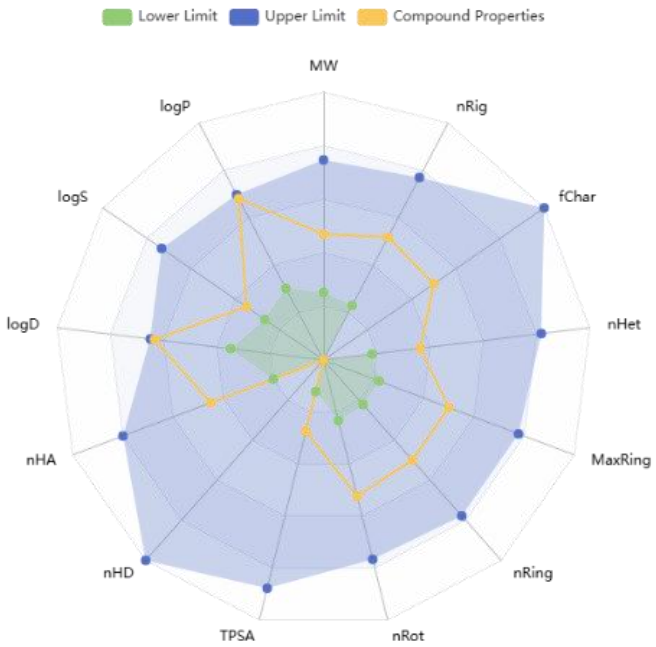
Lower Limit
Upper Limit
Compound Properties
MW
nRig
fChar
nHet
MaxRing
nRing
nRot
TPSA
nHD
nHA
logD
logS
logP

3f

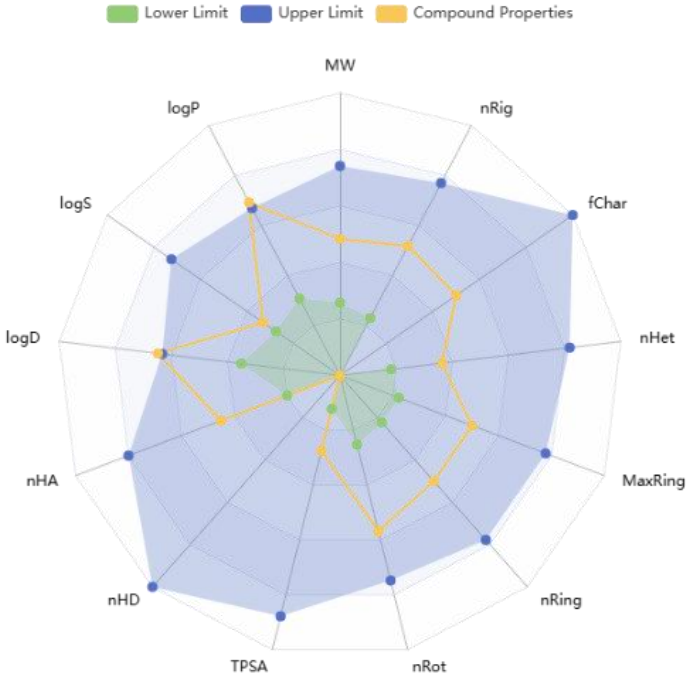
Lower Limit
Upper Limit
Compound Properties
MW
nRig
fChar
nHet
MaxRing
nRing
nRot
TPSA
nHD
nHA
logD
logS
logP

3g

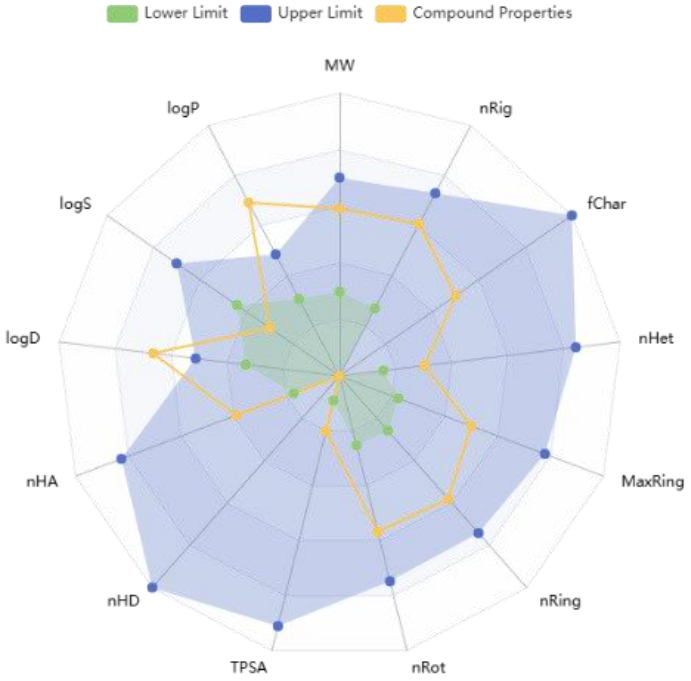
Lower Limit
Upper Limit
Compound Properties
MW
nRig
fChar
nHet
MaxRing
nRing
nRot
TPSA
nHD
nHA
logD
logS
logP

3h

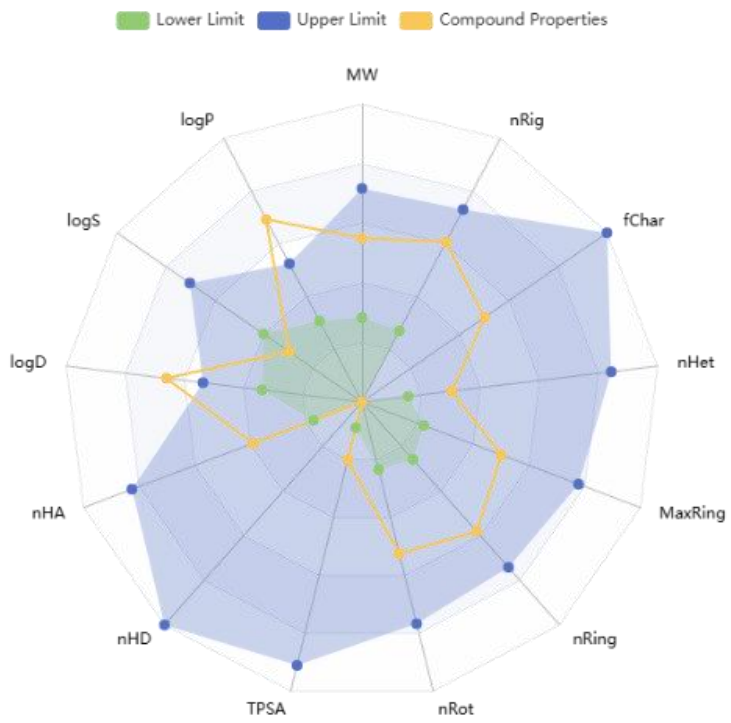

3i

Figure 6: Generated radar plots of 3a-i NHC complexes

Additional detailed ADMET data for the PEPPSI-Pd(II)-NHC complexes **3a-i** are available in the PDF supporting file for comprehensive reference.

Docking analysis

The docking study evaluated the binding affinities of nine brominated heterocyclic compounds (3a to 3i) with two proteins: 4IQK (Keap1 Kelch domain, associated with healthy lung cells, BEAS2B) and 6GUE (CDK2, linked to colon cancer cells, HCT116). The proteins were prepared by removing water and adding polar hydrogens using PyMOL, followed by docking simulations conducted with the HDOCK server [79-82], which is primarily designed for protein-protein interactions but adapted here for small molecules. This approach aimed to assess the potential of these compounds as selective anticancer agents by examining their interactions with cancer-related and healthy cell-associated proteins.

Docking Results for Keap1 (4IQK)

The results from Table 10 revealed that all compounds exhibited strong binding to Keap1, with docking scores ranging from -190.22 to -211.96 and confidence scores between 0.6909 and 0.7754. The CAS residues, such as Arg415 and Ser508, aligned with the known Nrf2

binding site, validating the docking accuracy for this protein. This strong interaction suggests that the compounds may influence the antioxidant response in healthy cells, which could be a drawback for their use as cancer-specific treatments, as it indicates potential toxicity to healthy lung cells.

Table 10 : HDOCK server docking results for compounds **3a-3i** with KEAP1 (4IQK) protein, including docking scores, confidence scores, peripheral anionic site (PAS) and catalytic active site (CAS) residues, and root mean square deviation (RMSD) values (å)

Compound	Docking score	Confidence score	PAS	CAS	RMSD
3a	-190.22	0.6909	TYR 334A, SER 363A, TYR 525A	ARG 415A, ARG 483A, SER 508A, GLY 509A	59.89
3b	-193.12	0.7032	TYR 334A, SER 363A, TYR 525A	ARG 415A, ARG 483A, SER 508A, GLY 509A	60.14
3c	-211.96	0.7754	TYR 334A, SER 363A, TYR 525A	ARG 415A, ARG 483A, SER 508A, GLY 509A	60.07
3d	-197.90	0.7227	TYR 334A, SER 363A, TYR 525A	ARG 415A, ARG 483A, SER 508A, GLY 509A	59.22
3e	-193.23	0.7036	TYR 334A, SER 363A, TYR 525A	ARG 415A, ARG 483A, SER 508A, GLY 509A	59.00
3f	-206.23	0.7548	TYR 334A, SER 363A, TYR 525A	ARG 415A, ARG 483A, SER 508A, GLY 509A	59.94
3g	-207.72	0.7603	TYR 334A, SER 363A, TYR 525A, HIS 575A	ARG 415A, ARG 483A, SER 508A, GLY 509A	60.25
3h	-192.18	0.6992	TYR 334A, PHE 335A, ARG 336A, TYR 572A	ARG 415A, ARG 483A, SER 555A, TYR 525A	60.90
3i	-205.74	0.7530	TYR 334A, TYR 572A, HIS 575A, and PHE 577A	ARG 415A, ARG 483A, SER 555A, and TYR 525A	59.81

Docking Results for CDK2 (6GUE)

In contrast, the data from Table 11 showed weaker binding to CDK2, with docking scores ranging from -129.04 to -136.57 and lower confidence scores from 0.3967 to 0.4333. The CAS residues identified, such as Ser264 and His268, did not correspond to the standard CDK2 active site (Lys33, Glu81, Asp86, Asp145), suggesting that the compounds may bind to non-catalytic sites. This raises concerns about their effectiveness as CDK2 inhibitors, which are typically targeted for cancer cell cycle disruption, potentially limiting their anticancer potential.

Table 11: HDOCK server docking results for compounds **3a-3i** with CDK2/CYCLINA (6GUE) protein, including docking scores, confidence scores, peripheral anionic site (PAS) and catalytic active site (CAS) residues, and root mean square deviation (RMSD) values (å)

Compound	Docking score	Confidence score	PAS	CAS	RMSD
3a	-130.55	0.4040	TYR 269A, ARG 260A, SER 261A, LEU 219A, LEU 267A, ILE 275A, SER 249A	SER 264A, HIS 268A, PHE 248A, VAL 226A, ARG 245A, LYS 273A, GLN 265A	51.08
3b	-131.41	0.4081	LEU 219A, SER 249A, SER 261A, GLN 265A, LEU 267A, TYR 269A, ILE 275A	VAL 226A, ARG 245A, PHE 248A, ARG 260A, SER 264A, HIS 268A, LYS 273A	51.31
3c	-136.57	0.4333	ILE 275A, PHE 152A, PRO 155A, ALA 277A, ASN 272A, ARG 122A, ILE 186A, HIS 121A, VAL 154A	ALA 116A, HIS 119A, SER 120A, SER 181A, THR 182A, ALA 183A, PRO 271A, ARG 274A, LYS 278A, SER 276A, VAL 156A	40.95
3d	-131.04	0.4063	ILE 275A, PHE 152A, PRO 155A, ALA 277A, ASN 272A, ARG 122A,	ALA 116A, HIS 119A, SER 120A, SER 181A, THR	39.94

			ILE 186A, HIS 121A, VAL 154A	182A, ALA 183A, PRO 271A, ARG 274A, LYS 278A, SER 276A, VAL 156A	
3e	-129.04	0.3967	ILE 275A, PHE 152A, PRO 155A, ALA 277A, ASN 272A, ILE 186A, ARG 122A, HIS 121A, VAL 154A	ALA 116A, HIS 119A, SER 120A, SER 181A, THR 182A, ALA 183A, PRO 271A, ARG 274A, LYS 278A, SER 276A, VAL 156A	39.68
3f	-135.31	0.4271	PHE 152A, PRO 155A, ALA 277A, ASN 272A, ILE 186A, ARG 122A, HIS 121A, VAL 154A	ALA 116A, HIS 119A, SER 120A, SER 181A, THR 182A, ALA 183A, PRO 271A, ARG 274A, LYS 278A, SER 276A, ILE 275A, VAL 156A	40.72
3g	-133.22	0.4169	PHE 203A, PRO 253A, PRO 204A, ILE 215A, VAL 252A, ALA 194A	ALA 201A, ARG 200A, ARG 214A, ARG 217A, THR 198A, THR 218A, GLN 246A, LEU 202A, LYS 250A, TRP 243A, VAL 251A	48.16
3h	-135.00	0.4256	LEU 219A, ARG 260A, ILE 275A, SER 261A, ARG 274A	SER 264A, HIS 268A, ARG 245A, TYR 269A, VAL 226A, LYS 273A, GLN 265A, PHE 248A, LEU 267A	51.36
3i	-130.85	0.4054	PHE 152A, PRO 155A, ALA 277A, ILE 186A, ASN 272A, VAL 154A,	ALA 116A, HIS 119A, SER 120A, SER 181A, THR	40.86

			ARG 122A, HIS 121A, ALA 279A	182A, ALA 183A, PRO 271A, ARG 274A, LYS 278A, SER 276A, ILE 275A, VAL 156A	

The correlation between docking and experimental data suggests that stronger Keap1 binding (higher negative docking score) may correlate with reduced toxicity to healthy cells, as seen with (**3c**), which showed no effect on BEAS2B. For cancer cells, the relationship is less clear; (**3c**) with a better CDK2 score had a moderate HCT116 IC_{50}, while (**3i**) with a weaker score had a lower IC_{50}, indicating other factors influence activity. This discrepancy highlights the need for further investigation into the compounds' mechanisms, as docking alone does not fully predict their selectivity or efficacy.The docking study indicates that compounds bind more strongly to Keap1 than CDK2, suggesting a potential bias toward affecting healthy cells, which could limit their use as selective anticancer agents. While the CAS residues for Keap1 align with known binding sites, the non-standard binding sites on CDK2 warrant further validation to confirm their relevance. Although experimental data for (**3c**) and (**3i**) show promise due to their varying effects on cancer and healthy cells, the lack of complete data across all compounds and the mismatch with docking sites mean more research is needed. These findings position 3c and **3i** as potential candidates for further development, but their optimization for selectivity remains a critical next step.

Conclusion

In summary, a new series of air- stable PEPPSI themed palladium(II) carbene complexes were synthesized and fully characterized by NMR spectroscopy, elemental analysis, Mass spectroscopy, and X- ray crystallography. The anticancer and antioxidant activities of the ligand and mixed ligand metal complexes were also investigated, with the latter showing favourable activities. Furthermore, the in vitro anticancer activity results indicated that, among the tested compounds, complex **3g** showed the highest cytotoxicity in SH-SY5Y cell line. IC_{50} value of this complex was 349.71 ± 30.04 against MCF-7 and HT-29 cells. The antioxidant capacity of the produced compounds was assessed using DPPH assays and compared to a positive control, Butylated hydroxytoluene (BHT) (50 ug/ml). Notably, palladium played a vital role in enhancing the biological activity against the selected human

cell lines. Further research is needed to elucidate their mechanism of action and evaluate their in vivo efficacy and safety profiles. DFT computations verified the complexes' geometric and electronic stability, with a HOMO-LUMO gap of 3.55–3.75 eV, while molecular docking revealed stronger binding to Keap1 (healthy cell model) than CDK2 (cancer target). ADMET profiling showed promising drug-likeness but flagged pharmacokinetic and toxicity issues, indicating a need for structural refinements to boost therapeutic potential.

Author contributions

Youssef arfaoui, Guerfi Samiaa, lamjed Mansour, Berredjem Yamina, Naceur Hamdi: conceptualization, methodology, writing, project administration, and funding acquisition; Donia Ben Salah and Mohamed Oussama Zouaghi: investigation, provision of access to various apparatuses and instruments; Naceur Hamdi: writing, and funding acquisition.

Declaration of conflicting interests

The author(s) declared no potential conflicts of interest with respect to the research, authorship, and/or publication of this article.

Data Availability

Data used to support the findings of this study are available from the corresponding author upon request.

Conflicts of Interest

The authors declare no conflicts of interest.

-Ethical Considerations, Consent to Participate, and Consent for Publication: Not applicable

Acknowledgements

The authors extended their appreciation to the Researchers Supporting Project number (RSP2025R75), King Saud University, Riyadh, Saudi Arabia

References

[1] L. Pauling, J. Chem. Soc. Chem. Commun. 1980, 15, 688.

[2] M. C. Jahnke, F. E. Hahn, From Laboratory Curiosities to Efficient Synthetic Tools. 2016.

[3] D. J. Nelson, S. P. Nolan, Chem. Soc. Rev. 2013, 42, 6723.

[4] W. A. Herrmann, Angew. Chem. Int. Ed. 2002, 41, 1290.

[5] M. S. Szulmanowicz, A. Gniewek, W. Gil, A. M. Trzeciak, ChemCatChem 2013, 5, 1152.

[6] R. A. Haque, N. Hasanudin, M. A. Iqbal, A. Ahmad, S. Hashim, A. M. S. Abdul Majid, M. B. K. Ahamed, J. Coord. Chem 2013, 66, 3211.

[7] J. P. Owings, N. N. McNair, Y. F. Mui, T. N. Gustafsson, A. Holmgren, M. Contel, J. R. Mead, FEMS Microbiol. Lett. 2016, 363, fnw148.

[8] A. T. Termaten, M. Schakel, A. W. Ehlers, M. Lutz, A. L. Spek, K. Lammertsma, Chem. Eur. J. Chem. A 2003, 9, 3577.

[9] L. Cavallo, A. Correa, C. Costabile, H. Jacobsen, J. Organomet. Chem. 2005, 69, 5407.

[10] X. Hu, I. Castro-Rodriguez, K. Meyer, J. Am. Chem. Soc. 2004, 126, 13464.

[11] F. Glorius, F. Glorius, N-Heterocyclic Carbenes in Transition Metal Catalysis. Topics in Organometallic Chemistry 2007, 1–20.

[12] M. Regitz, Angew. Chem. Int. Ed. Engl. 1996, 35, 725.

[13] H. J. Hao, D. F. Chen, W. Zhang, X. Li, K. F. Wang, J. Y. Lei, L. F. Tang, J. Coord. Chem. 2024, 1.

[14] Q. Teng, Y. Zhao, Y. Lu, Z. Liu, H. Chen, D. Yuan, Q. Meng, Organometallics 2022, 41, 161.

[15] S. Budagumpi, B. K. Narayana, R. S. Keri, N. D. Hanumantharayudu, M. Vijayakumar, P. Viswanathamurthi, Appl. Organomet. Chem. 2023, 37, 7225.

[16] N. Iqbal, M. Yaqoob, M. Javed, M. Abbasi, J. Iqbal, M. A. Iqbal, Comput. Theor. Chem. 2021, 1197, 113.

[17] S. Y. Hussaini, R. A. Haque, M. R. Razali, J. Organomet. Chem. 2019, 882, 96.

[18] U. Tutar, C. Çelik, E. Üstün, N. Özdemir, N. Şahin, D. Sémeril, İ. Özdemir, Inorganics 2023, 11, 385.

[19] N. Şahin, G. Serdaroğlu, S. D. Düşünceli, M. N. Tahir, C. Arıcı, İ. Özdemir, J. Coord. Chem. 2019, 72, 3258.

[20] C. J. O'Brien, E. A. B. Kantchev, C. Valente, N. Hadei, G. A. Chass, A. Lough, M. G. Organ, Chem. Eur. J. Chemistry A 2006, 12, 4743.

[21] O. Hollóczki, Chem.-A Eur. J. 2020, 26, 4885.

[22] N. Sakander, A. Ahmed, B. Rasool, D. Mukherjee, An Overview of NHeterocyclic Carbene: Properties and Applications, Intechopen, 2023, 147.

[23] M. N. Hopkinson, C. Richter, M. Schedler, F. Glorius, Nature 2014, 510, 485.

[24] H. Jacobsen, A. Correa, A. Poater, C. Costabile, L. Cavallo, Coord. Chem. Rev. 2009, 253, 687.

[25] J. Lund, H. F. Jónsson, A. Fiksdahl, Results in Chem. 2022, 4, 100360.

[26] S. D. Dusunceli, M. H. Sahan, M. Kaloglu, E. Ustun, I. Ozdemir, J. Chin. Chem. Soc. 2022, 69, 1937.

[27] F. Li, J. J. Hu, L. L. Koh, T. A. Hor, Dalton Trans. 2010, 39, 5231.

[28] F. E. Hahn, M. C. Jahnke, V. Gomez-Benitez, D. Morales-Morales, T. Pape, Organometallics 2005, 24, 6458.

[29] J. F. Hartwig, M. Kawatsura, S. I. Hauck, K. H. Shaughnessy, L. M. AlcazarRoman, J. Org. Chem. 1999, 64, 5575.

[30] M. G. Organ, G. A. Chass, D. C. Fang, A. C. Hopkinson, C. Valente, Synthesis 2008, 2008, 2776.

[31] S. Shi, P. Lei, M. Szostak, Organometallics 2017, 36, 3784

[32] P. Nun, J. Martinez, F. Lamaty, Synlett 2009, 2009, 1761.

[33] I. Al Nasr, N. Touj, W. Koko, T. Khan, I. Özdemir, S. Yaşar, N. Hamdi, Catalysts 2020, 10, 1190.

[34] W. Liu, R. Gust, Chem. Soc. Rev. 2013, 42(2), 755.

[35] S. Akkoç, V. Kayser, İ. Ö. İlhan, D. E. Hibbs, Y. Gök, P. A. Williams, B. Hawkins, F. Lai, J. Organomet. Chem. 2017, 839, 98.

[36] S. Akkoç, İ. Özer İlhan, Y. Gök, P. J. Upadhyay, V. Kayser, Inorg. Chim. Acta 2016, 449, 75.

[37] T. Scattolin, E. Bortolamiol, S. Palazzolo, I. Caligiuri, T. Perin, V. Canzonieri, N. Demitri, F. Rizzolio, L. Cavallo, B. Dereli, M. V. Mane, S. P. Nolan, F. Visentin, ChemComm 2020, 56(81), 12238.

[38] G. Dahm, C. Bailly, L. Karmazin, S. Bellemin- Laponnaz, Organomet. Chem. 2015, 794, 115.

[39] F. Türker, C. Gürses, D. Barut Celepci, A. Aktaş, B. Ateş, Y. Gök, Arch. Pharm. 2019, 352(12), 1900187.

[40] F. Erdemir, D. Barut Celepci, A. Aktaş, Y. Gök, R. Kaya, P. Taslimi, Y. Demir, İ. Gulçin, Bioorg. Chem. 2019, 91, 103134.

[41] F. Türker, S. Abbas, A. Noma, A. Aktaş, K. Al- Khafaji, T. Taşkın Tok, B. Ateş, Y. Gök, Monatsh. Chem. 2020, 151, 1557.

[42] 1228 S. Daşgın, Y. Gök, D. Barut Celepci, P. Taslimi, M. İzmirli, A. Aktaş, İ. Gulcin, J. Mol. Struct. 2020, 1228, 129442.

[43] S. Bal, Ö. Demirci, B. Şen, P. Taslimi, A. Aktaş, Y. Gök, M. Aygün, I. Gülçin, Polyhedron 2021, 198, 115060

[44] Ott I. Inorganic and organometallic transition metal complexes with biological molecules and living cells chapter five – medicinal chemistry of metal N-heterocyclic carbene (NHC) complexes. Academic Press; 2017.

[45] Askunowo PO, Haque RA, Razali MR. A comparative insight into the bioactivity of mono- and binuclear silver(I)-N-heterocyclic carbene complexes: synthesis, lipophilicity and substituent effect. Rev Inorg Chem 2017; 37: 29–50.

[46] Hahn FE, Jahnke MC. Heterocyclic carbenes heterocyclic carbenes: synthesis and coordination chemistry. Angew Chem Int Ed 2008 ; 47: 3122–72.

[47] Garino C, Gobetto R, Nervi C, Salassa L, Rosenberg E, Ross JBA, et al. Spectroscopic and computational studies of a Ru(II) terpyridine complex: the importance of weak intermolecular forces to photophysical properties. Inorg Chem 2007; 46: 8752–62.

[48] Temiz-Arpacı Ö, Arısoy M, Sac D, Doganc F, Tasci M, Şenol FS, et al. Biological evaluation and docking studies of some benzoxazole derivatives as inhibitors of acetylcholinesterase and butyrylcholinesterase. Z Naturforsch C J Biosci 2016;71: 409–13

[49] Özdemir İ, Çiftçi O, Evren E, Gürbüz N, Kaloğlu N, Türkmen NB, et al. Synthesis, characterization and antitumor properties of novel silver(I) and gold(I) N-heterocyclic carbene complexes. Inorg Chim Acta 2020; 506:119530–8

[50] G. Bitencourt- Ferreira, W. F. de Azevedo, Molegro Virtual Docker for Docking Docking Screens for Drug Discovery, Humana, New York, NY 2019, p. 149.

[51] S. Kusumaningrum, E. Budianto, S. Kosela, W. Sumaryono, F. Juniarti, J. Appl. Sci. 2014, 4, 47.

[52] X. Y. Meng, H. X. Zhang, M. Mezei, M. Cui, Curr. Comput.- Aided Drug Des. 2011, 7, 146.

[53] Stoe & Cie, X-AREA (Version 1.18) and X-RED32 (Version 1.04), Stoe & Cie, Darmstadt, Germany, 2002.

[54] G.M. Sheldrick, *SHELXT – Integrated space-group and crystal-structure determination*, Acta Crystallogr. Sect. A 71(1) (2015) 3−8.

[55] G.M. Sheldrick, *Crystal structure refinement with SHELXL*, Acta Crystallogr. Sect. C 71(1) (2015) 3−8.

[56] O.V. Dolomanov, L.J. Bourhis, R.J. Gildea, J.A.K. Howard, H. Puschmann, *OLEX2: a complete structure solution, refinement and analysis program*, J. Appl. Crystallogr. 42(2) (2009) 339−341.

[57] a) Hamdi, N.; Slimani, J.; Mansour, L.; Alresheedi, F.; Gürbüz, N.; Özdemir,I. N-heterocyclic carbene-palladium complexes and their catalytic activity in the direct C-H bond activation of heteroarene derivatives with aryl bromides: synthesis, and antimicrobial and antioxidant activities. *New J. Chem.* 2021, *45*, 21248-21262.b) Donia Bensalah, Lamjed Mansour, Mathieu Sauthier, Nevin Gurbuz,de Ismail Ozdemir, Lotfi Beji, Rafik Gatri and

Naceur Hamdi, Plausible PEPPSI catalysts for direct C–H functionalization of five-membered heterocyclic bioactive motifs: synthesis, spectral, X-ray crystallographic characterizations and catalytic activity, *RSC Adv*.**,** 2023,13, 31386-31410.

[58] M.G. Organ, G.A. Chass, D.C. Fang, A.C. Hopkinson, C. Valente, Pd-NHC (PEPPSI) complexes: synthetic utility and computational studies into their reactivity, Synthesis 17 (2008) 2776–2797.

[59] Almallah, H.; Brenner, E.; Matt, D.; Harrowfield, J.; Jahajh, M.; Hijazi, A. Palladium complexes of N-heterocyclic carbenes displaying an unsymmetrical N-alkylfluorenyl/N'-aryl substitution pattern and their behaviour in Suzuki– Miyaura cross coupling. *Dalton Trans* **2019**, *48*, 14516-14529.

[60] Muniyappan, N.; Sabiah, S. Synthesis, structure, and characterization of picolyl- and benzyl-linked biphenyl palladium N-heterocyclic carbene complexes and their catalytic activity in acylative cross-coupling reactions. *Appl. Organomet. Chem.*, **2020**, *34*, e5421.

[61] Guo, S.; Huynh, H. V. Dinuclear triazole-derived, Janus-type N-heterocyclic carbene complexes of palladium: Syntheses, isomerizations, and catalytic studies toward direct C5-arylation of imidazoles. *Organometallics*, **2014**, *33*, 2004-2011.

[62] Yang, L.; Powell, D-R.; Houser, R-P.; Structural variation in copper(i) complexes with pyridylmethylamide ligands: structural analysis with a new four-coordinate geometry index, τ4.
Dalton Trans., 2007, 955-964

[63] Serpe, A.; Pilia, L., Balestri, D.; Marchio, L.; Deplano, P.; Characterization and Structural Insights of the Reaction Products by Direct Leaching of the Noble Metals Au, Pd and Cu with N,N-Dimethyl-piperazine-2,3-dithione/I2 Mixtures. *Molecules*, **2021**, 26(16), 4721.

[64] Lasmari, S.; Gurbuz, N.; Boulcina, R.; Özdemir, N.; Özdemir, I. Synthesis of [PdBr2(benzimidazole-2-ylidene)(pyridine)] complexes and their catalytic activity in the direct CAH bond activation of 2-substituted heterocycles. *Polyhedron*. **2021,** 199, 115091.

[65] Ulu, O-D.; Serin, S.; Özdemir, N.; Özdemir, I.; Synthesis, crystal structure, and DFT studies of NHC mediated Pd-PEPPSI complex: Application for Suzuki reaction. *J. Mol. Struct.* **2025**, 1320, 139479.

[66] McKenzie, C. F.; Spackman, P. R.; Jayatilaka, D.; Spackman, M. A. *CrystalExplorer* model energies and energy frameworks: extension to metal coordination compounds, organic salts, solvates and open-shell systems, *IUCrJ*, **2017**, *4*, 575–587.

[67] Spackman, P. R.; Turner, M. J.; McKinnon, J. J.; Wolff, S. K.; Grimwood, D. J.; Jayatilaka, D.; Spackman, M. A. *Crystal Explorer 21.5*, University of Western Australia, Perth, Australia, **2021**.

[68] Spackman, M. A.; Jayatilaka, D. Hirshfeld Surface Analysis. *CrystEngComm*, **2009**, 11 (1), 19–32.

[69] Ryhl, T. Thermodynamic properties of palladium(II) chloride and bromide complexes in aqueous solution. *Acta Chem. Scand.* **1972**, *26*, 2961-2962.

[70] Hohenberg, P. ; Kohn, W. Inhomogeneous electron gas. *Phys. Rev.* **1964,** 136 (3B), 864.

[71] Kohn W.; Sham L. J. Phys. Rev. 140, A1133 – Published 15 November 1965.)

[72] Becke, B. D. Density-functional thermochemistry. III. The role of exact exchange, The Journal of Chemical Physics. **1993**, 98, 5648–5652.

[73] Stephens, P. J.; Devlin, F. J.; Chabalowski, C. F.; Frisch, M. J. Ab Initio Calculation of Vibrational Absorption and Circular Dichroism Spectra Using Density Functional Force Fields, J. Phys. Chem**. 1994**, 98, 11623–11627.

[74] Zouaghi, M.O.; Arfaoui, Y.; Champagne, B.; Density functional theory investigation of the electronic and optical properties of metallo-phthalocyanine derivatives, Opt. Mater. **2021,** 120, 113315.

[75] P. Jeffrey Hay; Willard R. Wadt, Ab initio effective core potentials for molecular calculations. Potentials for K to Au including the outermost core orbitals, J. Chem. Phys. **1985**, 822, 299-310.

[76] Ben Salah, D. ; Zouaghi, M. O. ; Hassen S. ; Arfaoui,Y. ;, Mansour, L.; Al-Quraishy S. Özdemir N.; N Gurbuz N. ; Özdemir, I.; Sauthier M. ; Hamdi, N. Inorganica Chimica Acta. **2025**, 574, 122398.

[77] Gaussian 16, Revision C.01, Frisch, M. J.; Trucks, G. W.; Schlegel, H. B.; Scuseria, G. E.; Robb, M. A.; Cheeseman, J. R.; Scalmani, G.; Barone, V.; Petersson, G. A.; Nakatsuji, H.; Li, X.; Caricato, M.; Marenich, A. V.; Bloino, J.; Janesko, B. G.; Gomperts, R.; Mennucci, B.; Hratchian, H. P.; Ortiz, J. V.; Izmaylov, A. F.; Sonnenberg, J. L.; Williams-Young, D.; Ding, F.; Lipparini, F.; Egidi, F.; Goings, J.; Peng, B.; Petrone, A.; Henderson, T.; Ranasinghe, D.; Zakrzewski, V. G.; Gao, J.; Rega, N.; Zheng, G.; Liang, W.; Hada, M.; Ehara, M.; Toyota, K.; Fukuda, R.; Hasegawa, J.; Ishida, M.; Nakajima, T.; Honda, Y.; Kitao, O.; Nakai, H.; Vreven, T.; Throssell, K.; Montgomery, J. A., Jr.; Peralta, J. E.; Ogliaro, F.; Bearpark, M. J.; Heyd, J. J.; Brothers, E. N.; Kudin, K. N.; Staroverov, V. N.; Keith, T. A.; Kobayashi, R.; Normand, J.; Raghavachari, K.; Rendell, A. P.; Burant, J. C.; Iyengar, S. S.; Tomasi, J.; Cossi, M.; Millam, J. M.; Klene, M.; Adamo, C.; Cammi, R.; Ochterski, J. W.; Martin, R. L.; Morokuma, K.; Farkas, O.; Foresman, J. B.; Fox, D. J. Gaussian, Inc., Wallingford CT, 2016.

[78] Balasundram, N., Sundram, K., & Samman, S. (2006). Phenolic compounds in plants and agri-industrial by-product : antioxidant activity, occurrence; and potential uses. Food Chemistry, 9, 191 – 120

[79] Y. Yan, H. Tao, J. He, S-Y. Huang, The HDOCK server for integrated protein-protein docking. Nature Protocols, **2020**, 15, 1829-1852.

[80] Y. Yan, D. Zhang, P. Zhou, B. Li, S-Y. Huang, HDOCK: a web server for protein-protein and protein-DNA/RNA docking based on a hybrid strategy. Nucleic Acids Res., **2017**, 45(W1): W365-W373.

[81] Y. Yan, Z. Wen, X. Wang, S-Y. Huang, Addressing recent docking challenges: A hybrid strategy to integrate template-based and free protein-protein docking, Proteins, **2017**, 85, 497-512.

[82] S-Y. Huang, X. Zou, A knowledge-based scoring function for protein-RNA interactions derived from a statistical mechanics-based iterative method, Nucleic Acids Res., **2014**;42(7), e55.